

Fractional-statistics-induced entanglement from Andreev-like tunneling

Gu Zhang¹, Pierre Glidic², Frédéric Pierre², Igor Gornyi³,
Yuval Gefen⁴

¹Beijing Academy of Quantum Information Sciences, Beijing 100193,
China.

²Université Paris-Saclay, CNRS,
Centre de Nanosciences et de Nanotechnologies, 91120 Palaiseau, France.

³Institute for Quantum Materials and Technologies and Institut für
Theorie der Kondensierten Materie, Karlsruhe Institute of Technology,
76131 Karlsruhe, Germany.

⁴Department of Condensed Matter Physics, Weizmann Institute of
Science, Rehovot 761001, Israel.

Contributing authors: frederic.pierre@c2n.upsaclay.fr;
igor.gornyi@kit.edu; yuval.gefen@weizmann.ac.il;

Abstract

The role of anyonic statistics stands as a cornerstone in the landscape of topological quantum techniques. While recent years have brought forth encouraging and persuasive strides in detecting anyons, a significant facet remains unexplored, especially in view of connecting anyonic physics to quantum information platforms—whether and how entanglement can be generated by anyonic braiding. Here, we demonstrate that even if the two anyonic subsystems are connected only by electron tunneling, anyonic entanglement, manifesting fractional statistics, is generated. Specifically, we address this question for fractional quantum Hall edges bridged by a quantum point contact that allows only transmission of fermions (so-called Andreev-like tunneling), invoking the physics of two-beam collisions in an anyonic Hong-Ou-Mandel collider. We define an entanglement pointer—a current-noise-based function tailored to quantify entanglement and show that it reflects the role of *quasiparticle statistics*. A striking feature of our statistics-induced-entanglement pointer is its relative resilience to entanglement stemming from electrostatic interactions between the two anyonic subsystems.

Keywords: Anyonic statistics, Andreev-like tunneling, entanglement

1 Introduction

One of the most fascinating classes of quasiparticles is known as anyons. These quasiparticles, defying conventional exchange statistics, are predicted to reside in topologically intricate states, e.g., those realized in the regime of fractional quantum Hall (FQH) effect [1, 2]. In particular, anyonic quasiparticles are hosted by the edges of Laughlin quantum-Hall states. Furthermore, the landscape of anyons extends to encompass Majorana modes, foreseen to materialize at the edges of topological superconducting materials [3, 4]. Recent years have borne witness to an intensified spotlight on anyons within the condensed-matter community. The focal point of this scrutiny stems from the pivotal role that exotic anyonic statistics should play in quantum technology. Over two decades have passed since the pioneering confirmation of the fractional charge of Laughlin quasiparticles [5, 6]. Inspired by earlier endeavors in the exploration of fractional statistics (see e.g., Refs. [7–9], most recently, highly persuasive signals of anyonic statistics have been directly or indirectly observed in Fabry–Perot [10–13] and Hong-Ou-Mandel interferometers [14–17].

This boost of progress in the quest for anyonic statistics is accompanied by a series of exhilarating experiments that have unveiled a plethora of exotic anyonic features in FQH systems. Among these observations are the existence of charge neutral modes [18, 19], fractional Josephson relation [20], and Andreev-like tunneling [15, 21–25] in an anyonic system [26]. What is particularly striking is the agreement between the experimental findings and their theoretical predictions. This alignment not only emboldens our understanding but also invigorates the search for further pathways to identify and comprehend anyons. Indeed, in addition to earlier theoretical ideas [27–38], most recently, there has been another surge of theoretical proposals [39–48] on understanding and detecting anyonic features, and possibly harnessing them for quantum information processing platforms (see, e.g., Refs. [49–52]).

Entanglement is another fundamental quantum mechanical element and a prerequisite for the development of quantum technology platforms. Despite its significance, experimentally quantifying entanglement remains a challenging endeavor, often entailing intricate considerations specific to each case. Recently, Ref. [53] proposed to measure entanglement stemming from quantum statistics of quasiparticles by a certain combination of the current cross-correlation functions. Following Ref. [53], the statistics-induced entanglement (i) showcases resilience against disruptions introduced by interactions, rendering it more robust in real-world scenarios, (ii) targets the genuine quantum entanglement that can be assessed through Bell-inequality [54] measurements (cf. Ref. [55]), and (iii) establishes a possibility of directly measuring the von Neumann entanglement entropy in transport experiments, thus deepening the understanding of entanglement manifestations. Experimental validation in integer quantum Hall systems lends further weight to these advantages [53].

However, when transitioning to anyonic systems, the quantification of entanglement becomes even more formidable, which is accentuated by the absence of readily available fractional statistics in natural environments. Furthermore, the quasiparticle collisions that can directly reveal the anyon’s statistics [34] in entanglement are now commonly believed to be irrelevant (e.g., Refs. [36, 38, 42, 46]) for the current-noise

measurements in anyonic Hong-Ou-Mandel colliders [14–16]. Nevertheless, the measurement of anyons’ entanglement through their collisions holds immense potential for the identification of anyons. Despite the importance of anyonic statistics in quantum techniques and the recent advances in the research of anyons, to date, the observation and quantification of anyonic statistics-induced entanglement remained a challenge.

2 Entanglement pointer for Andreev-like tunneling

In this work, we combine anyonic statistics and quantum entanglement, and define the *entanglement pointer* to quantify the statistics-induced entanglement in a Hong-Ou-Mandel interferometer on FQH edges with filling factor ν (Fig. 1a). The model at hand is crucially distinct from more conventional anyonic colliders [14–16, 36, 46] in that its central quantum point contact (QPC) only allows transmission of fermions [23, 25, 26]. The dilute non-equilibrium currents in the middle arms consist of anyons with charge νe (Fig. 1b), where ν is the filling fraction. Since only electrons are allowed to tunnel across the central QPC, such a tunneling event must be accompanied by leaving behind (“reflection”) a fractional hole of charge $-(1 - \nu)e$; the latter continues to travel along the original middle edge (Fig. 1c). Such a “reflection” event is reminiscent of the reflection of a hole in an orthodox Andreev tunneling from a normal metal to a superconductor; hence, such an event is commonly dubbed “quasiparticle Andreev reflection” [22]. As distinct from the conventional normal metal-superconductor case, in an anyonic Andreev-like tunneling process, (i) both the incoming anyon and reflected “hole” carry fractional charges, and (ii) the absolute values of anyonic and hole charges are different.

We divide the system into two subsystems \mathcal{A} and \mathcal{B} see Fig. 1a. To characterize the statistics-induced entanglement between these two parts, we introduce the *entanglement pointer* [53] for the Andreev-like tunneling:

$$\mathcal{P}_{\text{Andreev}} \equiv \frac{S_{\text{T}}(T_A, 0) + S_{\text{T}}(0, T_B) - S_{\text{T}}(T_A, T_B)}{eI_+}. \quad (1)$$

Here, $S_{\text{T}}(T_A, T_B)$ refers to the noise of tunneling current between two subsystems, as a function of corresponding “bare” transmission probabilities T_A and T_B of the two diluters, and T_C stands for the transmission probability at the central QPC that couples the subsystems. The entanglement pointer effectively subtracts out redundant contributions present when only one of the two sources is biased. The current $I_+ = I_{A0} + I_{B0}$ is a sum of non-equilibrium currents I_{A0} and I_{B0} in arm A and B (see Fig. 1a), respectively.

Although we have defined the entanglement pointer through the tunneling-current noise, it can also be measured with the cross-correlation noise, see Eq. (5) below and the ensuing discussion. Importantly, following its definition, $\mathcal{P}_{\text{Andreev}}$ excludes the single-source contributions and contains only noise from the two-particle collisions. For anyons, such processes are expected to involve braiding, so that $\mathcal{P}_{\text{Andreev}}$ should be capable of displaying anyonic statistics, an intrinsic feature of anyons. For $\mathcal{P}_{\text{Andreev}}$ to quantify statistics-induced entanglement, we need it to be robust against unwanted effects related to interaction along the middle channels. This is shown in

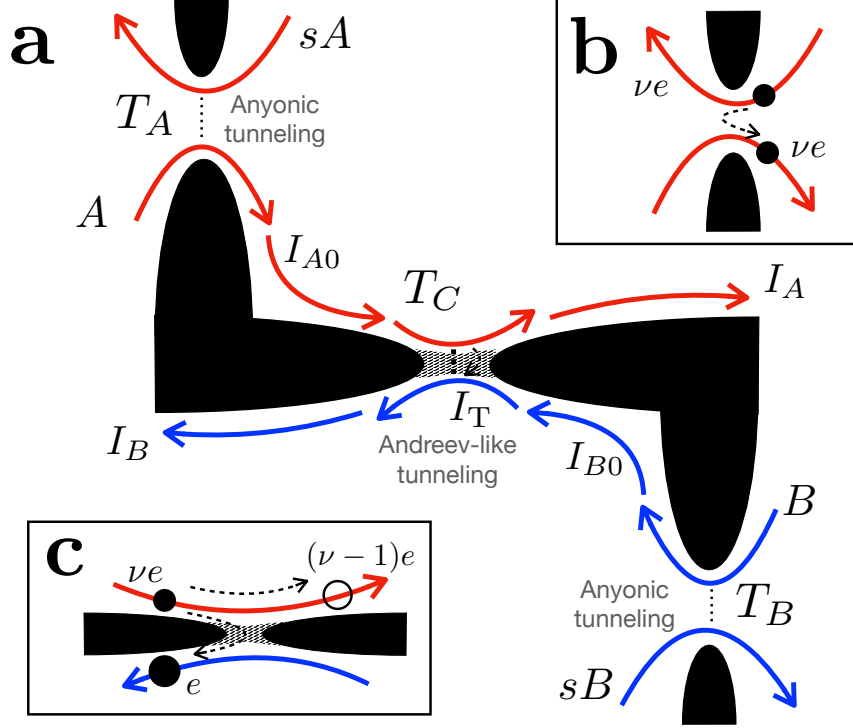


Fig. 1 Schematic depiction of the model with Andreev-like tunneling between the fractional edges (cf. Fig. S2 in the Supplementary Information). The quantum Hall droplets correspond to white regions separated by barriers (“fingers” introduced by gates) shown in black, the gray areas correspond to tunneling barriers for electrons (impenetrable for anyons). **a**, The entire setup consists of two sources (sA , sB) and two middle arms (A , B) in the FQH regime. They host chiral anyons that correspond to the bulk filling factor $\nu < 1/2$. Edge-state transport directions are designated with the red and blue curves, for subsystems \mathcal{A} (including sA and A) and \mathcal{B} (sB and B), respectively. I_A and I_B represent the currents in middle arms (A and B , respectively), after the central QPC. Before the central QPC, currents in arms A and B are instead represented by I_{A0} and I_{B0} , respectively. Current I_T tunnels through the central QPC, from arm A to arm B . **b**, Anyons with charge νe tunnel from the sources to corresponding middle arms A and B through diluters with transmissions T_A and T_B , respectively. **c**, Channels A and B communicate through the central quantum point contact (QPC) with the transmission T_C . Central QPC allows only electrons to tunnel (highlighted by the gray-shaded QPC), leading to the “reflection” of an anyonic hole [with charge $(\nu - 1)e$], resembling the Andreev reflection at the metal-superconductor interfaces.

Supplementary Information (SI). On a technical side, the evaluation of $\mathcal{P}_{\text{Andreev}}$ within the Keldysh framework involves both “connected” and “disconnected” diagrams (cf, Secs. IA and IB of the SI). This distinguishes our work from Ref. [48], where only “connected” diagrams were considered (only for a single-source setting, where anyonic collisions are not present).

3 Tunneling current noise

Before moving to the analysis of the tunneling-current noise, we would like to emphasize a crucial feature of the correlation functions determining the noise [Eq. (8) of Methods]: the separation of the non-equilibrium contributions. The non-equilibrium noise is, in turn, split into a single-source [the product of equilibrium and non-equilibrium terms in Eq. (8)] and double-source contributions (the product of non-equilibrium terms). The time integrals in all terms are dominated by ultraviolet contributions (cf, Sec. IC of the SI), which greatly contrasts the situation of anyonic tunneling. It is worth noting that this separation did not occur for self-contracted anyonic pairs in Refs. [36, 46]. Indeed, the resummation procedures employed in Refs. [36, 46] involve only dominant processes where non-equilibrium anyons form into self-contracted pairs, with which the double-source contribution distinguishes from a simple product of single-source ones only by a modification of the infrared cutoff. Collisions and braiding of two non-equilibrium anyons were thus neglected for the anyonic-tunneling setup in Refs. [16, 36, 42, 46].

For Andreev-like transmission through the central QPC, the expression for the tunneling noise can be decomposed as follows: $S_T = S_{1A} + S_{1B} + S_2$, where

$$S_{1A,1B} = T_C \frac{T_{A,B}}{\pi^2} \frac{2\nu \sin^2(\pi\nu) eI_{A0,B0}}{(2 - 3\nu + 2\nu^2)(2 - 4\nu + 2\nu^2)} \quad (2)$$

are single-source noises for sources sA , sB , respectively, and

$$S_2 = T_C \frac{T_A T_B}{\pi^2} \frac{2\nu \sin^2(\pi\nu) eI_+}{(2 - 5\nu + 4\nu^2)(2 - 6\nu + 4\nu^2)} \quad (3)$$

is the double-source ‘‘collision contribution’’ ($\nu < 1/2$ is assumed) (cf, Sec. I of the SI). Following Eq. (1), the entanglement pointer is proportional to S_2 , and, after removing the dependence on I_+ , reads

$$\mathcal{P}_{\text{Andreev}} = \frac{T_A T_B T_C}{\pi^2} \frac{2\nu \sin^2(\pi\nu)}{(2 - 5\nu + 4\nu^2)(2 - 6\nu + 4\nu^2)}. \quad (4)$$

The entanglement pointer, $\mathcal{P}_{\text{Andreev}}$, has two advantages over a single tunneling current noise. Firstly, $\mathcal{P}_{\text{Andreev}}$ reflects the statistics-induced extra Andreev-like tunneling for two-anyon collisions. It provides an alternative option (other than the braiding phase [10] and two-particle bunching or anti-bunching preferences [34]) to disclose anyonic statistics. For $0 < \nu < 1/2$, $\mathcal{P}_{\text{Andreev}}$ is positive, meaning that when two anyons collide at the central QPC, they prefer to promote Andreev-like tunnelings. Secondly, $\mathcal{P}_{\text{Andreev}}$ has a better resilience against interactions than the current noise. Indeed, with interactions, processes with only self-contracted pairs, which vanish for the non-interacting scenario, can become dominant in the tunneling current noise in the strongly diluted limit. This interaction-induced contribution is however removed in $\mathcal{P}_{\text{Andreev}}$ (cf. Sec. III of the Supplementray Information). Nevertheless, when evaluating $\mathcal{P}_{\text{Andreev}}$, interactions between the arms A and B slightly renormalize (through

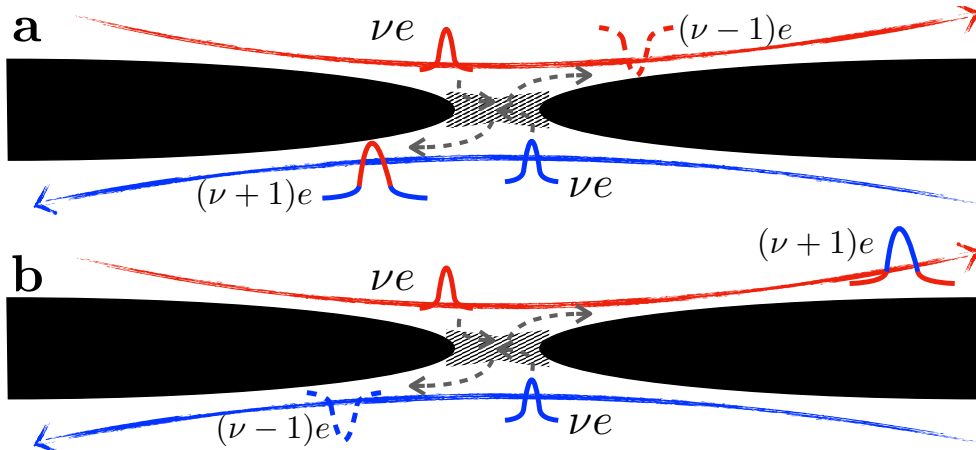


Fig. 2 Andreev-like tunneling processes for two anyons simultaneously arriving at the central QPC: Andreev-like tunneling produces fractional charges along both arms, in contrast to that of the single-anyon situation (cf. Fig. 1c).

interaction-induced fractionalization, see e.g., Ref. [21]) the statistical factors determined by ν in the two-particle terms (see Refs. [44, 45] for a discussion of scaling dimensions vs. anyonic phases in related setups).

4 Interpretation of entanglement pointer

The essence of entanglement pointer can be illustrated by resorting to single-particle (Fig. 1c) and two-particle (Fig. 2) scattering formalism revealing the statistical properties of anyons in the course of two-particle collisions. We emphasize that the picture of scattering of non-equilibrium anyons does not apply to Refs. [16, 36, 42, 46]. Indeed, these works consider only the correlations (“braiding”) of non-equilibrium anyons with the *equilibrium* excitations at the central QPC. The entanglement pointer $\mathcal{P}_{\text{Andreev}}$ is designed to capture only contributions of scattering events involving two non-equilibrium particles, through which particle statistics is manifested.

For models where the central QPC allows “intrinsic” non-equilibrium carriers (i.e., fermions for integer, or anyons for FQH edges) to tunnel, the influence of two-particle scatterings is manifested by their bunching or anti-bunching preference [34]. For the model under consideration, two-particle scattering instead influences the probability of Andreev-like tunneling events. To see this more clearly, we denote by W_A and W_B the probabilities (determined by the diluters and proportional to T_A and T_B) that an anyon from the corresponding source participates in the scattering at the central QPC. With this convention, a two-anyon scattering occurs with the probability $W_A W_B$. Andreev-like tunneling produces then fractional charges on both arms, as shown in Fig. 2. After including both single-particle and two-particle scattering events,

we obtain the differential noises at a given voltage V (cf, Sec. IV of the SI):

$$\begin{aligned}
s_T &= (s_T)_{\text{single}} + (s_T)_{\text{collision}} \\
&= (W_A + W_B)W_C - (W_A^2 + W_B^2)W_C^2 + W_A W_B P_{\text{Andreev}}^{\text{stat}} \\
s_{AB} &= (s_{AB})_{\text{single}} + (s_{AB})_{\text{collision}} \\
&= -(1 - \nu)W_C(W_A + W_B) - W_C(\nu - W_C)(W_A^2 + W_B^2) - W_A W_B P_{\text{Andreev}}^{\text{stat}},
\end{aligned} \tag{5}$$

where $s_T = \partial_{I_+} S_T$, $s_{AB} = \partial_{I_+} S_{AB}$ are the differential noises, and $S_{AB} = \int dt \langle \delta \hat{I}_A(t) \delta \hat{I}_B(0) \rangle$ is the irreducible zero-frequency cross-correlation (where $\delta \hat{I}_{A,B} \equiv \hat{I}_{A,B} - I_{A,B}$ refers to the fluctuation of the current operator $\hat{I}_{A,B}$), and subscripts “single” and “collision” indicate contributions from single-particle and two-particle scattering events, respectively. Here W_C refers to the transmission probability of an Andreev-like tunneling $W_C \propto T_C$. The factor $P_{\text{Andreev}}^{\text{stat}}$, which is proportional to the entanglement pointer $\mathcal{P}_{\text{Andreev}}$, refers to extra Andreev-like tunneling induced by anyonic statistics. It would be equal to zero if anyons from subsystem \mathcal{A} were distinguishable from those in \mathcal{B} . In this case, the noise would be equal to the sum of two single-source ones. By comparing to Eq. (4), W_A , W_B , W_C , and $P_{\text{Andreev}}^{\text{stat}}$ can be expressed via the microscopic parameters (cf, Secs. I and VI of the SI); in particular, $W_{A,B} = \partial_V I_{A0,B0} h / (e^2 \nu)$ are directly related to $G_{A,B}$ from Eq. (10). As another feature of Andreev-like tunnelings, S_T in Eq. (5) does not explicitly depend on ν , since the central QPC allows only charge e particles to tunnel.

Equation (5) discloses several features of Andreev-like tunneling in an anyonic model. Firstly, in the strongly diluted limit, $s_{AB} \approx (\nu - 1)s_T$, when considering only the leading contributions to the noise, i.e., the terms linear in both W_A (or W_B) and W_C . Both $(s_T)_{\text{single}}$ and $(s_{AB})_{\text{single}}$ correspond to S_{1A} or S_{1B} in Eq. (3) and will be removed following our definition of the entanglement pointer Eq. (1). In both functions, the double-source contributions, i.e., the bilinear terms $\propto W_A W_B$, involve $P_{\text{Andreev}}^{\text{stat}}$ – exactly the difference generated by statistics, when two anyons collide at the central QPC. Most importantly, bilinear terms of both functions of Eq. (5) have the same magnitude, i.e., $(s_T)_{\text{collision}} = -(s_{AB})_{\text{collision}}$. Consequently, the experimental measurement of $\mathcal{P}_{\text{Andreev}}$, though defined with tunneling current noise, can be performed by measuring the cross-correlation of currents in the drains, which is more easily accessible in real experiments:

$$\begin{aligned}
\mathcal{P}_{\text{Andreev}} &= W_A W_B \int d\epsilon P_{\text{Andreev}}^{\text{stat}}(\epsilon) / I_+ \\
&= \frac{S_{AB}(T_A, T_B) - S_{AB}(T_A, 0) - S_{AB}(0, T_B)}{e I_+}.
\end{aligned} \tag{6}$$

5 Comparison to experiment

We now compare the theoretical prediction with the experimental data from Ref. [25], see Fig. 3. Panel **a** shows the raw data for the double-source noise S_{AB} and for the sum of single-source S_{AB} . For the single-source data, the x -axis of Panel **a** represents

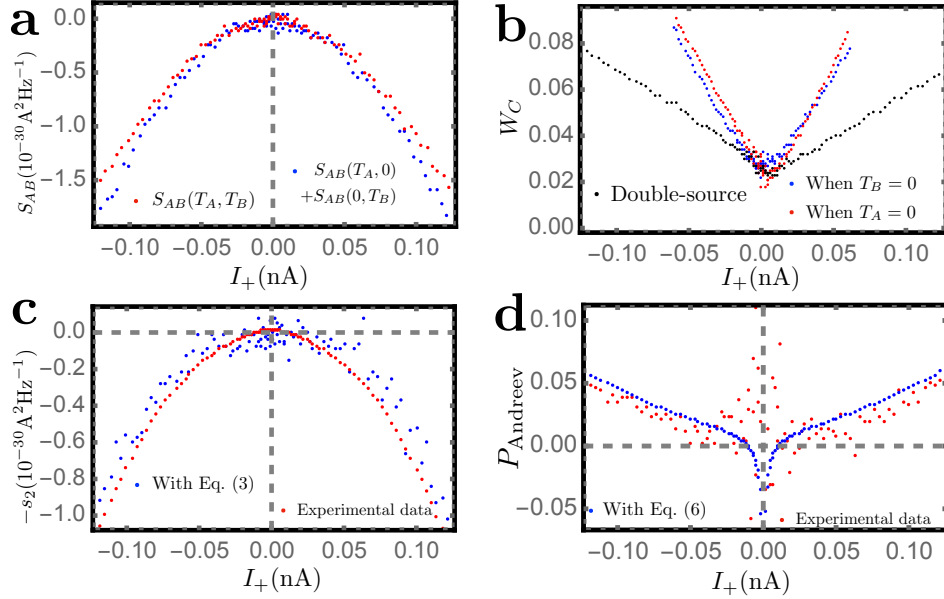


Fig. 3 The experimental data and comparison to the theory. **a**, The measured double-source (the red dots) and summation of single-source (the blue dots) S_{AB} , as a function of the total non-equilibrium current I_+ . **b**, The measured Andreev tunneling transmission W_C at the central QPC, for double-source (black dots) and single-source (red and blue dots) situations. **c**, The value of $-S_2$, obtained from Eq. (3) (the blue dots) and the difference between experimentally measured S_{AB} (the red dots). To obtain the latter one, we have rescaled the double-source S_{AB} , to compensate for the difference of T_C , shown in **b**, between double and single-source scenarios. **d**, Presents $\mathcal{P}_{\text{Andreev}}$ that corresponds to two scenarios of $-S_2$ shown in **c**.

$I_{A0}(T_A, 0) + I_{B0}(0, T_B)$, i.e., the sum of non-equilibrium current in two single-source situations. In contrast to the theoretical result Eq. (5), the double-source S_{AB} in Fig. 3a has a smaller amplitude than the sum of single-source ones. This fact is explained by the different values of the transmission T_C of the central QPC for the single-source and double-source cases, as shown in Fig. 3b, indicating a non-local influence of the voltage sources on T_C . To remove this electrostatic effect, we take the single-source transmission as the reference, to rescale the double-source S_{AB} (see SI for details), leading to S_2 of Fig. 3c. The rescaled data is further compared to that evaluated from S_2 of Eq. (3). The corresponding entanglement pointer, $\mathcal{P}_{\text{Andreev}}$, is presented in Fig. 3d. These plots demonstrate good agreement between the theory and experiment for both S_2 and $\mathcal{P}_{\text{Andreev}}$.

6 Conclusions

In this work, we have defined the entanglement pointer in an anyonic (with filling factor $\nu < 1/2$) Hong-Ou-Mandel interferometer that allows Andreev-like tunneling through the central QPC. The entanglement pointer and associated noise functions

are obtained by considering non-equilibrium anyon-triggered Andreev-like tunneling and “braiding” between reflected anyonic charges and non-equilibrium anyons that do not tunnel at the central QPC. The obtained entanglement pointer is a universal function of the filling factor ν (assuming vanishing interaction between arms of the two subsystems). In the presence of interactions along arms and across the QPCs, the entanglement pointer is anticipated to be highly resilient, as it involves the statistical phase gained by two-anyon scattering. The Andreev-like tunneling in an anyonic collider is “halfway” from the integer case of Ref. [53] (where both tunneling and dynamics along the arms are fermionic) to purely anyonic colliders (both tunneling and dynamics are anyonic). The latter case will be addressed elsewhere, with insights from the present work suggesting that quasiparticle collisions do matter in the collider geometry, (in contrast to a commonplace belief stipulating that anyonic collider dynamics is dominated by time-domain braiding [36, 38, 42, 46]). This provides us with a convenient setup for a direct inspection and study of real (non-virtual) anyonic collisions. We compare the theory predictions with the experiment. The measured data agrees remarkably well with the theoretically calculated one, for both S_{AB} and $\mathcal{P}_{\text{Andreev}}$. We have thus demonstrated the crucial role of two-particle scattering—collisions—in establishing fractional-statistics-induced entanglement in anyonic colliders.

While preparing our manuscript we have noticed Ref. [48], which concerns a single source platform. Technically, the analysis of Ref. [48] involves only connected diagrams. We note that the present analysis consists of (i) the inclusion of double-source noise, (ii) the designed entanglement pointer, as well as its resilience against interaction (cf, Sec. III of the SI), and (iii) “braiding” between reflected anyonic holes and non-equilibrium anyons.

7 Methods

7.1 Theoretical model

We consider the anyonic setup shown in Fig. 1a, which consists of two source arms (sA , sB) and two middle ones (A , B). The system is viewed as comprising two subsystems, \mathcal{A} (including sA and A) and \mathcal{B} (sB and B). The system Hamiltonian contains the three parts: $H = H_{\text{arms}} + H_{\text{diluter}} + H_{\text{T}}$. The arms, carrying charge- νe quasiparticles, can be described by the bosonized edge Hamiltonian $H_{\text{arms}} = v_F \sum_{\alpha} \int dx [\partial_x \phi_{\alpha}(x)]^2 / 4\pi$, with ϕ_{α} the bosonic field labeled by $\alpha = sA, sB, A, B$. Fractional charges tunnel from sources to middle arms through the quantum-Hall bulk at two QPCs. These two “diluter” QPCs are described by the Hamiltonian $H_{\text{diluter}} = \zeta_A \psi_A^{\dagger} \psi_{sA} + \zeta_B \psi_B^{\dagger} \psi_{sB} + \text{H.c.}$. Via bosonization, tunneling operators can be written as $\psi_{\alpha}^{\dagger} \psi_{\alpha'} = F_{\alpha}^{\dagger} F_{\alpha'} \exp[i\sqrt{\nu}(\phi_{\alpha'} - \phi_{\alpha})] / (2\pi a)$, with $F_{\alpha}^{\dagger} F_{\alpha'}$ the product Klein factors, and a an ultra-violet cutoff. The tunneling amplitudes ζ_A and ζ_B define the tunneling probabilities at the diluters, $T_A = |\zeta_A|^2$ and $T_B = |\zeta_B|^2$. The dynamical bosonic phase obeys the standard commutation relation $[\partial_x \phi_{\alpha}(x), \phi_{\beta}(x')] = i\pi \delta_{\alpha\beta} \delta(x-x')$. We assume strong dilution, $T_A, T_B \ll 1$. In this work, the same voltage bias V is assumed in both sources, and the single-source scenario is realized by pinching off either diluter.

The middle arms A and B communicate at the central QPC characterized by the transmission probability T_C . The central QPC is placed at a distance L from two

diluters, at the downstream transport direction [Fig. 1a]. In comparison to the two diluters, where the two depletion gates (the black area in Fig. 1b) are well separated in space, the central QPC is in the opposite limit where the gates are almost “touching” each other (Fig. 1c). Following self-duality of tunneling through FQH QPCs (see, e.g., Refs. [56–58]), only fermionic tunneling is allowed in this limit. Physically, there is no bulk state with filling factor ν between the two arms (red and blue in Fig. 1), and, hence, between the subsystems \mathcal{A} and \mathcal{B} , at the central QPC. The tunneling is then described by the Hamiltonian $H_T = \zeta_C \Psi_A^\dagger \Psi_B + \text{H.c.}$, with $\zeta_C \propto \sqrt{T_C}$ and $\Psi_\alpha = F_\alpha \exp(i\phi_\alpha/\sqrt{\nu})/\sqrt{2\pi a}$. This bosonized expression contains $\sqrt{1/\nu}$ instead of $\sqrt{\nu}$ encountered above, which is a hallmark of electron tunneling in anyonic systems.

7.2 Correlation functions

The building blocks of the entanglement pointer are current correlators. Considering the Andreev-like transmission limit at the collider, $T_C \ll 1$, the noise of the current operator $\hat{I}_T = i\zeta_C \Psi_B^\dagger \Psi_A + \text{H.c.}$ is given by

$$S_T = v_F^2 e^3 T_C \int dt \left\langle \left\{ \Psi_B^\dagger(0) \Psi_A(0), \Psi_A^\dagger(t) \Psi_B(t) \right\} \right\rangle_{T_C=0}, \quad (7)$$

with $\{, \}$ denoting an anticommutator. Evaluation of S_T involves correlators $\langle \Psi_A^\dagger(t) \Psi_A(0) \rangle$ and $\langle \Psi_B^\dagger(t) \Psi_B(0) \rangle$ at the position of the central QPC. At zero temperature, these read:

$$\begin{aligned} \left. \begin{aligned} \langle \Psi_A^\dagger(t^-) \Psi_A(0^+) \rangle \\ \langle \Psi_B(t^-) \Psi_B^\dagger(0^+) \rangle \end{aligned} \right\} &= \frac{\tau_0^{\frac{1}{\nu}-1}}{2\pi v_F (\tau_0 + it)^{1/\nu}} \\ &\times \left\{ 1 + c_\nu \frac{it I_{A0,B0} e^{\pm i\nu e V t/\hbar}}{e^{(i\nu e V t/\hbar)2\nu-1}} \exp \left[- (1 - e^{\pm 2i\pi\nu}) \frac{I_{A0,B0} t}{\nu e} \right] \right\}, \end{aligned} \quad (8)$$

where $\tau_0 \equiv a/v_F$, $c_\nu = 2\pi^2/[\nu \sin(2\pi\nu)\Gamma(1-2\nu)]$ with Γ the Gamma function, and the signs $+$ and $-$ in the phase factors correspond to A and B , respectively. In the strong-dilution limit, the non-equilibrium currents read as

$$I_{A0,B0} = G_{A,B}(V) V, \quad (9)$$

$$G_{A,B} = T_{A,B} \frac{(\nu e)^2}{2\pi^2 \hbar} \sin(2\pi\nu) \Gamma(1-2\nu) \left(\frac{\nu e V \tau_0}{\hbar} \right)^{2\nu-2}, \quad (10)$$

with $G_{A,B}$ the non-equilibrium conductances affected by the “Luttinger renormalization” of diluters.

The correlators in Eq. (8) contain the equilibrium contribution (unity in the square brackets) and the non-equilibrium one, induced by the bias from the corresponding source. As bias is fixed in our setup, the single-source contribution is obtained by pinching off one of two diluters (i.e., by setting either T_A or T_B to zero). Experimentally, another option is to set one voltage bias as zero. To describe this situation

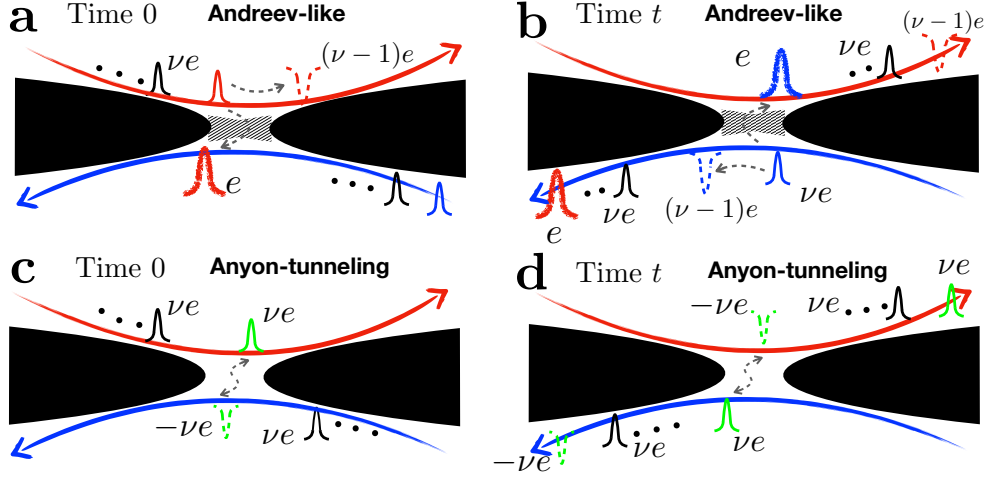


Fig. 4 Source of the exponential suppression of the non-equilibrium contribution in Eq. (8). Chiralities of arms are indicated by thick red and blue arrows, for upper and lower arms, respectively. Red and blue pulses denote non-equilibrium quasiparticles (in arms *A* and *B*, respectively) that Andreev-tunnel at the central QPC. Non-equilibrium anyons that do not Andreev-tunnel are instead indicated by black pulses. **a**, At time moment 0, an anyon from the upper channel triggers an Andreev-like tunneling, leaving a fractional hole (the inverted red dashed pulse) in the upper channel. **b**, At a later moment t , another fractional hole (the inverted blue dashed pulse) is created at the lower channel. These fractional holes produce a non-trivial phase by exchanging positions with other non-equilibrium pulses (the black ones). **c** and **d**, In comparison, for systems where anyons (rather than electrons) tunnel at the central QPC, leading processes [46] involve braiding of non-equilibrium anyons that do not tunnel at the central QPC (black pulses), and “vacuum bubbles” (green pulses) generated at moments 0 and t .

analytically, a finite temperature or finite system size must be included in Eqs. (8) and (10), to avoid the infrared divergence (see SI).

Similarly to non-interacting fermions (see, e.g., Refs. [59, 60]), connected diagrams that introduce the phase factor $\exp(i\nu e V t)$, are required for non-equilibrium contribution. Indeed, a non-equilibrium anyon is the prerequisite of Andreev-like tunneling. This connected diagram is, however, believed to be unimportant when anyons are allowed to tunnel at the central QPC. In Refs. [36, 42, 46], the so-called “bubble” diagrams [38] (i.e., self-contracted non-equilibrium anyon pairs) prevail over connected ones in the current noise calculated in the strongly diluted limit. Contributions from self-contracted anyonic pairs, however, vanish for Andreev-like tunneling to leading order in dilution, since exchanging positions of an anyon and an electron that tunnels at the central QPC produces only a trivial phase. This is in stark contrast to a non-trivial phase, $\pm\pi\nu$, which appears in the setups with anyonic tunneling at the central QPC, where it was interpreted as the anyonic “braiding” phase [43, 46].

In addition to an electron, a fractional hole (Fig. 1c) is also generated by the Andreev-like tunneling. As a quasiparticle with the fractional charge $(\nu - 1)e$, this hole can produce a non-trivial phase $\pm(\nu - 1)\pi$, when exchanging position with a non-equilibrium anyon. Consequently, when considering processes of higher-order in dilution or, equivalently, involving more non-equilibrium anyons (the black pulses in

Fig. 4), extra non-trivial phases will be produced by “braiding” non-equilibrium anyons and the fractional hole generated at the central QPC, at time moments 0 and t . After the resummation over such higher-order non-equilibrium processes, we obtain the exponential suppression factor $\exp\{-I_{A0,B0}t[1 - \exp(\pm 2i\pi\nu)]/\nu e\}$ in Eq. (8), which has the same structure as that in Refs. [16, 36, 43, 46] but involves anyonic holes produced from Andreev-like tunnelings, see Fig. 4.

7.3 Experiment

The measurements are realized at $T \approx 35$ mK on a 2DEG set to $\nu = 1/3$. The device includes two nominally identical source QPCs positioned symmetrically with respect to a central QPC (see SI and Ref. [25]). Gate voltages allow us to tune the QPCs in the configuration where the Andreev tunneling of quasiparticles takes place. The source QPCs are set in the anyonic-tunneling regime (Fig. 1b) and exhibit a shot noise Fano factor corresponding to a fractional charge $e^* \approx e/3$, whereas the central QPC is tuned in the Andreev-like tunneling regime (Fig. 1c) with the tunneling charge $e^* \approx e$, as deduced from shot noise [25]. An experimental challenge is to be able to obtain reliably the entanglement pointer. Indeed, $\mathcal{P}_{\text{Andreev}}$ is a small difference between larger quantities measured separately, which increases the sensitivity to experimental artifacts such as drifts in time between compared configurations or unwanted small capacitive cross-talks. As further detailed in the supplementary information, the data set presently used to extract the entanglement pointer was obtained following a specific protocol reducing such artifacts. In particular, there are no changes in the device gates voltages and the time between compared configurations is minimized. Further details on the experiment can be found in Sec. V of the SI.

Supplementary Information. In the Supplementary Information, we provide extra information on (i) detailed derivations of Eq. (8), on time-dependent correlation functions; (ii) finite-temperature expressions; (iii) influence of interaction on correlation functions and noises; (iv) Detailed derivation on single-particle and two-particle expressions, for different types of correlation functions; (v) more experimental information, and (vi) detailed information on the data analysis.

Acknowledgments. We are grateful to Gabriele Campagnano, Domenico Giuliano, Moty Heiblum, Thierry Martin, Bernd Rosenow, Inès Safi, and Kyrylo Snizhko for fruitful discussions. We thank O. Maillet, C. Piquard, A. Aassime, and A. Anthore for their contribution to the experiment. IG and YG acknowledge the support from the DFG grant No. MI658/10-2 and German-Israeli Foundation (GIF) grant No. I-1505-303.10/2019. YG acknowledges support from the Helmholtz International Fellow Award, by the DFG Grant RO 2247/11 – 1, by CRC 183 (project C01), the US-Israel Binational Science Foundation, and by the Minerva Foundation. FP acknowledges the support of the European Research Council (ERC-2020-SyG-951451) and of the French RENATECH network.

Declarations

- Conflict of interest: The authors declare no conflict of interest.

- Ethics approval: Not applicable
- Consent to participate: All coauthors participate in the preparation of this work.
- Consent for publication: All coauthors agree to publish this work.
- Availability of data and materials: Raw data of this work can be accessed via Zenodo: <https://doi.org/10.5281/zenodo.10434474>.
- Code availability: Relevant Mathematica notebook can be accessed via Zenodo: <https://doi.org/10.5281/zenodo.10434474>.
- Authors' contributions: GZ, IG, and YG carried out the theoretical analysis. PG obtained the experimental data and performed the low-level data analysis under the supervision of FP. GZ designed and performed the data-theory comparison, with critical inputs from FP. All authors participated in the scientific discussions, contributed to the preparation of this work and to the writing of the paper, and proofread the manuscript.

References

- [1] Laughlin, R.B.: Anomalous quantum Hall effect: An incompressible quantum fluid with fractionally charged excitations. *Phys. Rev. Lett.* **50**, 1395–1398 (1983) <https://doi.org/10.1103/PhysRevLett.50.1395>
- [2] Arovas, D., Schrieffer, J.R., Wilczek, F.: Fractional statistics and the quantum Hall effect. *Phys. Rev. Lett.* **53**, 722–723 (1984) <https://doi.org/10.1103/PhysRevLett.53.722>
- [3] Kitaev, A.Y.: Unpaired Majorana fermions in quantum wires. *Uspekhi Fizicheskikh Nauk (UFN)* **44**(10S), 131–136 (2001) <https://doi.org/10.1070/1063-7869/44/10s/s29>
- [4] Mong, R.S.K., Clarke, D.J., Alicea, J., Lindner, N.H., Fendley, P., Nayak, C., Oreg, Y., Stern, A., Berg, E., Shtengel, K., Fisher, M.P.A.: Universal topological quantum computation from a superconductor-Abelian quantum Hall heterostructure. *Phys. Rev. X* **4**, 011036 (2014) <https://doi.org/10.1103/PhysRevX.4.011036>
- [5] Saminadayar, L., Glattli, D.C., Jin, Y., Etienne, B.: Observation of the $e/3$ fractionally charged Laughlin quasiparticle. *Phys. Rev. Lett.* **79**, 2526–2529 (1997) <https://doi.org/10.1103/PhysRevLett.79.2526>
- [6] de-Picciotto, R., Reznikov, M., Heiblum, M., Umansky, V., Bunin, G., Mahalu, D.: Direct observation of a fractional charge. *Physica B: Condensed Matter* **249-251**, 395–400 (1998) [https://doi.org/10.1016/S0921-4526\(98\)00139-2](https://doi.org/10.1016/S0921-4526(98)00139-2)
- [7] Camino, F.E., Zhou, W., Goldman, V.J.: Realization of a Laughlin quasiparticle interferometer: Observation of fractional statistics. *Phys. Rev. B* **72**, 075342 (2005) <https://doi.org/10.1103/PhysRevB.72.075342>
- [8] Ofek, N., Bid, A., Heiblum, M., Stern, A., Umansky, V., Mahalu, D.: Role of interactions in an electronic Fabry–Perot interferometer operating in

the quantum Hall effect regime. Proceedings of the National Academy of Sciences **107**(12), 5276–5281 (2010) <https://doi.org/10.1073/pnas.0912624107>
<https://www.pnas.org/content/107/12/5276.full.pdf>

- [9] Willett, R.L., Nayak, C., Shtengel, K., Pfeiffer, L.N., West, K.W.: Magnetic-field-tuned Aharonov-Bohm oscillations and evidence for non-Abelian anyons at $\nu = 5/2$. Phys. Rev. Lett. **111**, 186401 (2013) <https://doi.org/10.1103/PhysRevLett.111.186401>
- [10] Nakamura, J., Fallahi, S., Sahasrabudhe, H., Rahman, R., Liang, S., Gardner, G.C., Manfra, M.J.: Aharonov–Bohm interference of fractional quantum Hall edge modes. Nature Physics **15**(6), 563–569 (2019) <https://doi.org/10.1038/s41567-019-0441-8>
- [11] Nakamura, J., Liang, S., Gardner, G.C., Manfra, M.J.: Direct observation of anyonic braiding statistics. Nature Physics **16**(9), 931–936 (2020) <https://doi.org/10.1038/s41567-020-1019-1>
- [12] Nakamura, J., Liang, S., Gardner, G.C., Manfra, M.J.: Impact of bulk-edge coupling on observation of anyonic braiding statistics in quantum Hall interferometers. Nature Communications **13**(1), 344 (2022) <https://doi.org/10.1038/s41467-022-27958-w>
- [13] Nakamura, J., Liang, S., Gardner, G.C., Manfra, M.J.: Fabry-Perot interferometry at the $\nu = 2/5$ fractional quantum Hall state (2023)
- [14] Bartolomei, H., Kumar, M., Bisognin, R., Marguerite, A., Berroir, J.-M., Bocquillon, E., Plaças, B., Cavanna, A., Dong, Q., Gennser, U., Jin, Y., Fève, G.: Fractional statistics in anyon collisions. Science **368**(6487), 173–177 (2020) <https://doi.org/10.1126/science.aaz5601>
- [15] Glidic, P., Maillet, O., Aassime, A., Piquard, C., Cavanna, A., Gennser, U., Jin, Y., Anthore, A., Pierre, F.: Cross-correlation investigation of anyon statistics in the $\nu = 1/3$ and $2/5$ fractional quantum Hall states. Phys. Rev. X **13**, 011030 (2023) <https://doi.org/10.1103/PhysRevX.13.011030>
- [16] Lee, J.-Y.M., Hong, C., Alkalay, T., Schiller, N., Umansky, V., Heiblum, M., Oreg, Y., Sim, H.-S.: Partitioning of diluted anyons reveals their braiding statistics. Nature **617**(7960), 277–281 (2023)
- [17] Ruelle, M., Frigerio, E., Berroir, J.-M., Plaças, B., Rech, J., Cavanna, A., Gennser, U., Jin, Y., Fève, G.: Comparing fractional quantum Hall Laughlin and Jain topological orders with the anyon collider. Phys. Rev. X **13**, 011031 (2023) <https://doi.org/10.1103/PhysRevX.13.011031>
- [18] Bhattacharyya, R., Banerjee, M., Heiblum, M., Mahalu, D., Umansky, V.: Melting of interference in the fractional quantum Hall effect: Appearance of neutral modes.

- Phys. Rev. Lett. **122**, 246801 (2019) <https://doi.org/10.1103/PhysRevLett.122.246801>
- [19] Dutta, B., Umansky, V., Banerjee, M., Heiblum, M.: Isolated ballistic non-abelian interface channel. *Science* **377**(6611), 1198–1201 (2022) <https://doi.org/10.1126/science.abm6571>
- [20] Kapfer, M., Roulleau, P., Santin, M., Farrer, I., Ritchie, D.A., Glattli, D.C.: A Josephson relation for fractionally charged anyons. *Science* **363**(6429), 846–849 (2019) <https://doi.org/10.1126/science.aau3539>
- [21] Safi, I., Schulz, H.J.: Transport in an inhomogeneous interacting one-dimensional system. *Phys. Rev. B* **52**, 17040–17043 (1995) <https://doi.org/10.1103/PhysRevB.52.R17040>
- [22] Sandler, N.P., Chamon, C.d.C., Fradkin, E.: Andreev reflection in the fractional quantum Hall effect. *Phys. Rev. B* **57**, 12324–12332 (1998) <https://doi.org/10.1103/PhysRevB.57.12324>
- [23] Hashisaka, M., Jonckheere, T., Akiho, T., Sasaki, S., Rech, J., Martin, T., Muraki, K.: Andreev reflection of fractional quantum Hall quasiparticles. *Nature Communications* **12**, 2794 (2021) <https://doi.org/10.1038/s41467-021-23160-6>
- [24] Cohen, L.A., Samuelson, N.L., Wang, T., Taniguchi, T., Watanabe, K., Zaltel, M.P., Young, A.F.: Universal chiral Luttinger liquid behavior in a graphene fractional quantum Hall point contact (2022)
- [25] Glidic, P., Maillet, O., Piquard, C., Aassime, A., Cavanna, A., Jin, Y., Gennser, U., Anthore, A., Pierre, F.: Quasiparticle Andreev scattering in the $\nu = 1/3$ fractional quantum Hall regime. *Nature Communications* **14**(1), 514 (2023) <https://doi.org/10.1038/s41467-023-36080-4>
- [26] Comforti, E., Chung, Y.C., Heiblum, M., Umansky, V., Mahalu, D.: Bunching of fractionally charged quasiparticles tunnelling through high-potential barriers. *Nature* **416**, 515–518 (2002) <https://doi.org/10.1038/416515a>
- [27] Safi, I., Devillard, P., Martin, T.: Partition noise and statistics in the fractional quantum Hall effect. *Phys. Rev. Lett.* **86**, 4628–4631 (2001) <https://doi.org/10.1103/PhysRevLett.86.4628>
- [28] Kane, C.L., Fisher, M.P.A.: Shot noise and the transmission of dilute Laughlin quasiparticles. *Phys. Rev. B* **67**, 045307 (2003) <https://doi.org/10.1103/PhysRevB.67.045307>
- [29] Vishveshwara, S.: Revisiting the Hanbury Brown–Twiss setup for fractional statistics. *Phys. Rev. Lett.* **91**, 196803 (2003) <https://doi.org/10.1103/PhysRevLett.91.196803>

- [30] Kim, E.-A., Lawler, M., Vishveshwara, S., Fradkin, E.: Signatures of fractional statistics in noise experiments in quantum Hall fluids. *Phys. Rev. Lett.* **95**, 176402 (2005) <https://doi.org/10.1103/PhysRevLett.95.176402>
- [31] Law, K.T., Feldman, D.E., Gefen, Y.: Electronic Mach-Zehnder interferometer as a tool to probe fractional statistics. *Phys. Rev. B* **74**, 045319 (2006) <https://doi.org/10.1103/PhysRevB.74.045319>
- [32] Feldman, D.E., Gefen, Y., Kitaev, A., Law, K.T., Stern, A.: Shot noise in an anyonic Mach-Zehnder interferometer. *Phys. Rev. B* **76**, 085333 (2007) <https://doi.org/10.1103/PhysRevB.76.085333>
- [33] Rosenow, B., Halperin, B.I.: Influence of interactions on flux and back-gate period of quantum Hall interferometers. *Phys. Rev. Lett.* **98**, 106801 (2007) <https://doi.org/10.1103/PhysRevLett.98.106801>
- [34] Campagnano, G., Zilberberg, O., Gornyi, I.V., Feldman, D.E., Potter, A.C., Gefen, Y.: Hanbury Brown–Twiss interference of anyons. *Phys. Rev. Lett.* **109**, 106802 (2012) <https://doi.org/10.1103/PhysRevLett.109.106802>
- [35] Campagnano, G., Zilberberg, O., Gornyi, I.V., Gefen, Y.: Hanbury Brown and Twiss correlations in quantum Hall systems. *Phys. Rev. B* **88**, 235415 (2013) <https://doi.org/10.1103/PhysRevB.88.235415>
- [36] Rosenow, B., Levkivskyi, I.P., Halperin, B.I.: Current correlations from a mesoscopic anyon collider. *Phys. Rev. Lett.* **116**, 156802 (2016) <https://doi.org/10.1103/PhysRevLett.116.156802>
- [37] Campagnano, G., Lucignano, P., Giuliano, D.: Chirality and current-current correlation in fractional quantum Hall systems. *Phys. Rev. B* **93**, 075441 (2016) <https://doi.org/10.1103/PhysRevB.93.075441>
- [38] Han, C., Park, J., Gefen, Y., Sim, H.-S.: Topological vacuum bubbles by anyon braiding. *Nature Communications* **7**(1), 11131 (2016) <https://doi.org/10.1038/ncomms11131>
- [39] Lee, B., Han, C., Sim, H.-S.: Negative excess shot noise by anyon braiding. *Phys. Rev. Lett.* **123**, 016803 (2019) <https://doi.org/10.1103/PhysRevLett.123.016803>
- [40] Rosenow, B., Stern, A.: Flux superperiods and periodicity transitions in quantum Hall interferometers. *Phys. Rev. Lett.* **124**, 106805 (2020) <https://doi.org/10.1103/PhysRevLett.124.106805>
- [41] Rech, J., Jonckheere, T., Grémaud, B., Martin, T.: Negative δ - T noise in the fractional quantum Hall effect. *Phys. Rev. Lett.* **125**, 086801 (2020) <https://doi.org/10.1103/PhysRevLett.125.086801>

- [42] Schiller, N., Shapira, Y., Stern, A., Oreg, Y.: Anyon statistics through conductance measurements of time-domain interferometry. *Phys. Rev. Lett.* **131**, 186601 (2023) <https://doi.org/10.1103/PhysRevLett.131.186601>
- [43] Morel, T., Lee, J.-Y.M., Sim, H.-S., Mora, C.: Fractionalization and anyonic statistics in the integer quantum Hall collider. *Phys. Rev. B* **105**, 075433 (2022) <https://doi.org/10.1103/PhysRevB.105.075433>
- [44] Schiller, N., Oreg, Y., Snizhko, K.: Extracting the scaling dimension of quantum Hall quasiparticles from current correlations. *Phys. Rev. B* **105**, 165150 (2022) <https://doi.org/10.1103/PhysRevB.105.165150>
- [45] Zhang, G., Gornyi, I.V., Spånslätt, C.: Delta- T noise for weak tunneling in one-dimensional systems: Interactions versus quantum statistics. *Phys. Rev. B* **105**, 195423 (2022) <https://doi.org/10.1103/PhysRevB.105.195423>
- [46] Lee, J.-Y.M., Sim, H.-S.: Non-Abelian anyon collider. *Nature Communications* **13**(1), 6660 (2022) <https://doi.org/10.1038/s41467-022-34329-y>
- [47] Jonckheere, T., Rech, J., Grémaud, B., Martin, T.: Anyonic statistics revealed by the Hong-Ou-Mandel dip for fractional excitations. *Phys. Rev. Lett.* **130**, 186203 (2023) <https://doi.org/10.1103/PhysRevLett.130.186203>
- [48] Iyer, K., Martin, T., Rech, J., Jonckheere, T.: Quasiparticle Andreev reflection in the Laughlin fractions of the fractional quantum hall effect. *Phys. Rev. B* **108**, 155404 (2023) <https://doi.org/10.1103/PhysRevB.108.155404>
- [49] Nielsen, M.A., Chuang, I.L.: *Quantum Computation and Quantum Information: 10th Anniversary Edition*. Cambridge University Press, Cambridge (2010). <https://doi.org/10.1017/CBO9780511976667>
- [50] Wilde, M.M.: *Quantum Information Theory*. Cambridge University Press, Cambridge (2013). <https://doi.org/10.1017/CBO9781139525343>
- [51] Nayak, C., Simon, S.H., Stern, A., Freedman, M., Das Sarma, S.: Non-Abelian anyons and topological quantum computation. *Rev. Mod. Phys.* **80**, 1083–1159 (2008) <https://doi.org/10.1103/RevModPhys.80.1083>
- [52] Alicea, J., Fendley, P.: Topological phases with parafermions: Theory and blueprints. *Annual Review of Condensed Matter Physics* **7**(1), 119–139 (2016) <https://doi.org/10.1146/annurev-conmatphys-031115-011336> <https://doi.org/10.1146/annurev-conmatphys-031115-011336>
- [53] Zhang, G., Hong, C., Alkalay, T., Umansky, V., Heiblum, M., Gornyi, I.V., Gefen, Y.: Measuring statistics-induced entanglement entropy with a Hong-Ou-Mandel interferometer (2022)

- [54] Bell, J.S.: On the Einstein-Podolsky-Rosen paradox. *Physics Physique Fizika* **1**, 195–200 (1964) <https://doi.org/10.1103/PhysicsPhysiqueFizika.1.195>
- [55] Chtchelkatchev, N.M., Blatter, G., Lesovik, G.B., Martin, T.: Bell inequalities and entanglement in solid-state devices. *Phys. Rev. B* **66**, 161320 (2002) <https://doi.org/10.1103/PhysRevB.66.161320>
- [56] Fendley, P., Ludwig, A.W.W., Saleur, H.: Exact nonequilibrium dc shot noise in Luttinger liquids and fractional quantum Hall devices. *Phys. Rev. Lett.* **75**, 2196–2199 (1995) <https://doi.org/10.1103/PhysRevLett.75.2196>
- [57] Shopen, E., Gefen, Y., Meir, Y.: Quasiparticle tunneling through a barrier in the fractional quantum Hall regime. *Phys. Rev. Lett.* **95**, 136803 (2005) <https://doi.org/10.1103/PhysRevLett.95.136803>
- [58] Weiss, U.: *Quantum Dissipative Systems*, 4th edn. World Scientific, Singapore (2012). <https://doi.org/10.1142/8334>
- [59] Bruus, H., Flensberg, K.: *Many-Body Quantum Theory in Condensed Matter Physics: An Introduction*, 2nd edn. Oxford University Press, London (2004)
- [60] Mahan, G.D.: *Many-particle Physics*. Springer, New York (2000)

Supplementary Information for “Statistics-induced entanglement generated by Andreev-like tunneling between fractional quantum Hall edges”

Gu Zhang, Pierre Glidic, Frédéric Pierre, Igor Gornyi, and Yuval Gefen
(Dated: December 27, 2023)

In this Supplementary Information, we provide details on (i) Time-dependent correlation functions of operators from each subsystem; (ii) Finite-temperature correlation functions; (iii) Influence of interactions, on the tunneling-current noise; (iv) Analysis on noises, with the picture of single-particle and two-particle scatterings; (v) Experimental details, and (vi) Details on the experiment-theory comparison.

I. Time-dependent correlation functions at zero temperature

In this section, we provide details of the derivation of Eq. (8) in the main text, i.e., correlation functions $\langle \Psi_A^\dagger(L, t) \Psi_A(L, 0) \rangle$ and $\langle \Psi_B^\dagger(L, t) \Psi_B(L, 0) \rangle$, for edges A and B , respectively. To the leading order of tunneling at the central QPC T_C , these two correlation functions are needed to obtain both tunneling current, and current noises.

IA. Leading-order correlations

We begin with expansions of the correlation functions to leading order in dilution $T_{A,B}$ at the corresponding diluter. **For simplicity, in this section we take $v_F = e = \hbar = 1$ during the derivation.** For concreteness, we focus on the correlation function of operators in edge A , i.e., $\langle \Psi_A^\dagger(L, t) \Psi_A(L, 0) \rangle$. After the leading-order expansion, the correlator is represented as a double time integral,

$$\begin{aligned}
 D_{A1} &\equiv -T_A \sum_{\eta_1 \eta_2} \eta_1 \eta_2 \iint ds_1 ds_2 e^{-i\nu V(s_1 - s_2)} \langle \Psi_A^\dagger(L, t^-) \Psi_A(L, 0^+) \psi_A^\dagger(0, s_1^{\eta_1}) \psi_A(0, s_2^{\eta_2}) \rangle \\
 &\quad \times \langle \psi_{sA}(0, s_1^{\eta_1}) \psi_{sA}^\dagger(0, s_2^{\eta_2}) \rangle \\
 &= \frac{-T_A}{(2\pi a)^3} \sum_{\eta_1 \eta_2} \eta_1 \eta_2 \iint ds_1 ds_2 \frac{e^{-i\nu V(s_1 - s_2)}}{(a + it)^{\frac{1}{\nu}} [a + i(s_1 - s_2) \chi_{\eta_1 \eta_2}(s_1 - s_2)]^{2\nu}} a^{\frac{1}{\nu} + 2\nu} \\
 &\quad \times \frac{[a + i(t - s_1 - L) \chi_{-\eta_1}(t - s_1)] [a + i(-s_2 - L) \chi_{+\eta_2}(-s_2)]}{[a + i(t - s_2 - L) \chi_{-\eta_2}(t - s_2)] [a + i(-s_1 - L) \chi_{+\eta_1}(-s_1)]},
 \end{aligned} \tag{S1}$$

where “A1” indicates the expansion to the leading order of T_A , s_1 and s_2 are the time moments when non-equilibrium anyons tunnel from sA to A , with η_1 and η_2 the corresponding Keldysh indexes. The function $\chi_{\eta\eta'}(t - t')$ reflects the relative positions of t^η and $t^{\eta'}$: it equals one if t^η is in front of $(t')^{\eta'}$ along the Keldysh contour, equals minus one for the opposite situation, and equals zero if $t = t'$ and $\eta = \eta'$. The

voltage bias is included in the phase factor $\exp[-i\nu V(s_1 - s_2)]$, with the standard transformation as introduced in, e.g., Ref. [S1].

In the main text, we comment that Eq. (S1) contains only the contribution from “connected” diagrams, i.e., Andreev-like tunneling (at the central QPC) triggered by an incoming non-equilibrium anyon. This process is addressed as “connected” in the main text, because of its similarity to tunnelings of non-interacting fermionic systems [S2, S3], where disconnected diagrams (addressed as “self-contracted anyonic pairs” in the main text) are known to vanish. Before moving to evaluation of connected diagrams, we pause for a while, to further clarify meanings of the terminologies: connected and disconnected diagrams. Briefly, these terms are introduced in non-interacting fermionic systems, where a disconnected diagram, corresponding to $s_1 \rightarrow s_2$, is exactly decomposable into two fully separated “sub-diagrams” that produce zero results for both current and noise. In anyonic systems, however, strictly speaking, diagrams corresponding to $s_1 \rightarrow s_2$ are not necessarily “disconnected”, due to possible (local or non-local) “braiding” between self-contracted non-equilibrium operators, and anyonic operators that tunnel at the central QPC. This is exactly the case when the central QPC allows anyons to tunnel [S4–S6], where non-equilibrium anyonic operators produce a non-trivial phase $\exp[i\pi\nu(\eta_1 - \eta_2)]$ when “braiding” with anyonic excitations at the central QPC. In this work, we however address the $s_1 \rightarrow s_2$ as disconnected, for the convenience of discussion.

Although important for anyonic tunneling at the central QPC, disconnected diagrams are irrelevant to Andreev-like tunnelings, to leading order in diluter transmission. Indeed, the last line of D_{A1} [Eq. (S1)] equals $\exp[i\pi(\eta_1 - \eta_2)] = 1$ when taking $s_1 \rightarrow s_2$, which indicates the absence of “braiding” (being “disconnected” in the physical sense) and yields a vanishing result after summations over Keldysh indexes η_1 and η_2 . The vanishing contribution of this leading disconnected diagram is fully reasonable, as a non-equilibrium anyon, from the physical point of view, is the prerequisite of an Andreev-like tunneling. Indeed, without an incoming non-equilibrium anyon, this system is effectively equivalent to two equilibrium edges connected by a QPC, where both anyonic and electronic tunneling processes are forbidden.

Now we move to evaluate the leading contribution from connected diagrams. Here, we use the identity (whose validity, as discussed in Ref. [S7], requires a much smaller bosonic short-time cutoff than the fermionic counterpart),

$$\frac{1}{(i\tau_0 - t)[i\tau_0\chi_{\eta_1\eta_2}(s_1 - s_2) - (s_1 - s_2)]} \frac{[i\tau_0\chi_{-\eta_1}(t - s_1) - (t - s_1 - L)][i\tau_0\chi_{+\eta_2}(-s_2) - (-s_2 - L)]}{[i\tau_0\chi_{-\eta_2}(t - s_2) - (t - s_2 - L)][i\tau_0\chi_{+\eta_1}(-s_1) - (-s_1 - L)]} \\ = \frac{1}{(i\tau_0 - t)[i\tau_0\chi_{\eta_1\eta_2}(s_1 - s_2) - (s_1 - s_2)]} + \frac{1}{[i\tau_0\chi_{-\eta_2}(t - s_2) - (t - s_2 - L)][i\tau_0\chi_{+\eta_1}(-s_1) - (-s_1 - L)]}, \quad (\text{S2})$$

to rewrite Eq. (S1) as

$$\begin{aligned}
& - \frac{T_A}{(2\pi\tau_0)^3} \sum_{\eta_1\eta_2} \eta_1\eta_2 \iint ds_1 ds_2 \frac{e^{-i\nu V(s_1-s_2)} [i\chi_{\eta_1\eta_2}(s_1-s_2)]^{2\nu} (i)^{1/\nu}}{(i\tau_0-t)^{1/\nu} [i\tau_0\chi_{\eta_1\eta_2}(s_1-s_2) - (s_1-s_2)]^{2\nu}} \tau_0^{\frac{1}{\nu}+2\nu} \\
& \times \frac{[i\tau_0\chi_{-\eta_1}(t-s_1) - (t-s_1-L)][i\tau_0\chi_{+\eta_2}(-s_2) - (-s_2-L)] \chi_{-\eta_2}(t-s_2)\chi_{+\eta_1}(-s_1)}{[i\tau_0\chi_{-\eta_2}(t-s_2) - (t-s_2-L)][i\tau_0\chi_{+\eta_1}(-s_1) - (-s_1-L)] \chi_{-\eta_1}(t-s_1)\chi_{+\eta_2}(-s_2)} \\
& = \frac{-T_A}{(2\pi\tau_0)^3} \sum_{\eta_1\eta_2} \eta_1\eta_2 \iint ds_1 ds_2 \frac{e^{-i\nu V(s_1-s_2)}}{(i\tau_0-t)^{1/\nu-1} [i\tau_0\chi_{\eta_1\eta_2}(s_1-s_2) - (s_1-s_2)]^{2\nu-1}} \tau_0^{\frac{1}{\nu}+2\nu} \\
& \times [i\chi_{\eta_1\eta_2}(s_1-s_2)]^{2\nu} (i)^{1/\nu} \frac{\chi_{-\eta_2}(t-s_2)\chi_{+\eta_1}(-s_1)}{\chi_{-\eta_1}(t-s_1)\chi_{+\eta_2}(-s_2)} \\
& \times \left\{ \frac{1}{(i\tau_0-t)[i\tau_0\chi_{\eta_1\eta_2}(s_1-s_2) - (s_1-s_2)]} + \frac{1}{[i\tau_0\chi_{-\eta_2}(t-s_2) - (t-s_2-L)][i\tau_0\chi_{+\eta_1}(-s_1) - (-s_1-L)]} \right\}, \tag{S3}
\end{aligned}$$

where τ_0 refers to the ultraviolet cutoff (in time). In Eq. (S3), first term of the last line corresponds to the “disconnected” diagram, which vanishes following our analysis above. After ignoring this “disconnected” contribution, we notice that as $\nu < 1/2$ (such that the red term is not singular), Eq. (S3) contains only two poles: $s_1 = -L$ and $s_2 = t - L$. We also notice that when $\nu > 1/2$, the red term contains the pole $s_1 \rightarrow s_2$ even after choosing the connected contribution [i.e., by taking the second term of the last line of Eq. (S3)]. This is actually the case for a non-interacting fermionic system. This complexity is, however, avoided by choosing $\nu < 1/2$, a satisfactory requirement for all Laughlin edge states. When considering only poles $s_1 = -L$ and $s_2 = t - L$, we are allowed to carry out the integral above by means of the contour integration, i.e.,

$$\int d(t-s_2) \frac{e^{-i\nu V(t-s_2)}}{i\tau_0\eta_2 - (t-s_2)} \int ds_1 \frac{e^{-i\nu V s_1}}{i\tau_0\eta_1 + s_1} = (\eta_2 - 1)(\eta_1 + 1)\pi^2, \tag{S4}$$

which indicates that only the option $\eta_1 = 1$ and $\eta_2 = -1$ is allowed, to obtain a finite result. These choices of Keldysh indexes are related to the fact that $V > 0$ pre-selects the allowed contour (i.e., upper or lower half of the complex plane) when performing the integral. With the integrated result, we obtain

$$D_{A1} = T_A e^{i\nu V t} \frac{1}{2\pi\tau_0^{3-\frac{1}{\nu}-2\nu}} \frac{1}{(\tau_0 + it)^{2\nu+1/\nu-2}}. \tag{S5}$$

We can combine D_{A1} with the equilibrium contribution given by

$$D_{A0} \equiv \tau_0^{\frac{1}{\nu}-1} (\tau_0 + it)^{-1/\nu} / 2\pi, \tag{S6}$$

and borrow the leading-order expression of the corresponding non-equilibrium current

$$I_{A0} = T_A \nu \tau_0^{2\nu-2} \sin(2\pi\nu) \Gamma(1-2\nu) (\nu V)^{2\nu-1} / 2\pi^2,$$

to arrive at

$$D_{A0} + D_{A1} = \frac{\tau_0^{\frac{1}{\nu}-1}}{2\pi(\tau_0 + it)^{1/\nu}} \left[1 + e^{i\nu V t} c(\nu) \frac{I_{A0}}{(\nu V)^{2\nu-1}} (it)^{2-2\nu} \right], \quad (\text{S7})$$

$$c(\nu) = \frac{2\pi^2}{\sin(2\pi\nu)\Gamma(1-2\nu)\nu}.$$

It is instructive to compare the $\nu \rightarrow 1$ limit of Eq. (S7), where $\lim_{\nu \rightarrow 1} c(\nu) = 2\pi$, with that of a non-interacting fermionic system: the latter has the correlation function

$$\langle \Psi_A^\dagger(t) \Psi_A(0) \rangle_{\text{fermion}} = \frac{1}{2\pi(\tau_0 + it)} (1 + e^{iVt} T_A - T_A). \quad (\text{S8})$$

After taking $\nu \rightarrow 1$, and $I_{A0}/V = 2\pi T_A$, we notice that the Eq. (S7) perfectly captures the first two terms of the non-interacting fermionic result, however, misses the last term. This missing term requires taking the $s_1 \rightarrow s_2$ pole (the one marked out in red) of Eq. (S3), after choosing the connected diagram [the second term of the last line of Eq. (S3)]. This term is absent in Eq. (S7), as the (to be integrated) function becomes regular when $\nu > 1/2$ for Laughlin quasiparticles.

IB. Processes of higher-order in dilution coefficients

Now we proceed to analyze the contribution of higher-order processes involving multiple non-equilibrium anyons that arrive at the central QPC between two Andreev-like tunneling events. As has been analyzed in the main text, these non-equilibrium anyons induce non-trivial phases, via ‘‘braiding’’ with fractional holes generated by Andreev-like tunnelings. In this section, we provide a detailed analysis to illustrate this point. We begin with the fourth-order term in the expansion of the correlation function in diluter tunneling amplitudes (second order in T_A):

$$\begin{aligned} D_{A2} &\equiv T_A^2 \frac{2^4}{4!} \sum_{\eta_1 \eta_2 \eta_3 \eta_4} \eta_1 \eta_2 \eta_3 \eta_4 \iint ds_1 ds_2 ds_3 ds_4 e^{-i\nu V (s_1 - s_2 + s_3 - s_4)} \\ &\quad \times \langle \psi_{sA}(0, s_1^{\eta_1}) \psi_{sA}^\dagger(0, s_2^{\eta_2}) \psi_{sA}(0, s_3^{\eta_3}) \psi_{sA}^\dagger(0, s_4^{\eta_4}) \rangle \\ &\quad \times \langle \Psi_A^\dagger(L, t^-) \Psi_A(L, 0^+) \psi_A^\dagger(0, s_1^{\eta_1}) \psi_A(0, s_2^{\eta_2}) \psi_A^\dagger(0, s_3^{\eta_3}) \psi_A(0, s_4^{\eta_4}) \rangle \\ &= \frac{T_A^2}{48\pi^5 \tau_0^5} \sum_{\eta_1 \eta_2 \eta_3 \eta_4} \eta_1 \eta_2 \eta_3 \eta_4 \iint ds_1 ds_2 ds_3 ds_4 e^{-i\nu V (s_1 - s_2 + s_3 - s_4)} \\ &\quad \times \langle e^{i\sqrt{\nu} \phi_{sA}(0, s_1^{\eta_1})} e^{-i\sqrt{\nu} \phi_{sA}(0, s_2^{\eta_2})} e^{i\sqrt{\nu} \phi_{sA}(0, s_3^{\eta_3})} e^{-i\sqrt{\nu} \phi_{sA}(0, s_4^{\eta_4})} \rangle \\ &\quad \times \langle e^{-\frac{i}{\sqrt{\nu}} \phi_A(L, t^-)} e^{\frac{i}{\sqrt{\nu}} \phi_A(L, 0^+)} e^{-i\sqrt{\nu} \phi_A(0, s_1^{\eta_1})} e^{i\sqrt{\nu} \phi_A(0, s_2^{\eta_2})} e^{-i\sqrt{\nu} \phi_A(0, s_3^{\eta_3})} e^{i\sqrt{\nu} \phi_{sA}(0, s_4^{\eta_4})} \rangle, \end{aligned} \quad (\text{S9})$$

which contains non-equilibrium operators taken at the four time moments: s_1, s_2, s_3 and s_4 . We assume that two out of four non-equilibrium vertexes contract with electron operators at the central QPC (corresponding to the connected diagram). The other two then have to perform self-contraction (the disconnected diagram). Without loss

of generality, we choose operators labeled as 3 and 4 (i.e., with time variables s_3, s_4 , and Keldysh indexes η_3, η_4) to have self-contraction. With this option, we can the last two lines of Eq. (S9) as

$$\begin{aligned}
& \frac{\tau_0^{2\nu+1/\nu}}{(\tau_0 + it)^{1/\nu-1} [\tau_0 + i(s_1 - s_2) \chi_{\eta_1 \eta_2}(s_1 - s_2)]^{2\nu-1}} \frac{\tau_0^{2\nu}}{[\tau_0 + i(s_3 - s_4) \chi_{\eta_3 \eta_4}(s_3 - s_4)]^{2\nu}} \\
& \times \frac{1}{[\tau_0 + i(t - s_2 - L) \chi_{-\eta_2}(t - s_2)] [\tau_0 + i(-s_1 - L) \chi_{+\eta_1}(-s_1)]} \\
& \times \frac{[\tau_0 + i(t - s_1 - L) \chi_{-\eta_1}(t - s_1)] [\tau_0 + i(-s_2 - L) \chi_{+\eta_2}(-s_2)]}{(\tau_0 + it) [\tau_0 + i(s_1 - s_2) \chi_{\eta_1 \eta_2}(s_1 - s_2)]} \\
& \times \frac{[\tau_0 + i(t - s_3 - L) \chi_{-\eta_3}(t - s_3)] [\tau_0 + i(-s_4 - L) \chi_{+\eta_4}(-s_4)]}{[\tau_0 + i(t - s_4 - L) \chi_{-\eta_4}(t - s_4)] [\tau_0 + i(-s_3 - L) \chi_{+\eta_3}(-s_3)]} \\
& \times \frac{[\tau_0 + i(s_1 - s_3) \chi_{\eta_1 \eta_3}(s_1 - s_3)]^{2\nu} [\tau_0 + i(s_2 - s_4) \chi_{\eta_2 \eta_4}(s_2 - s_4)]^{2\nu}}{[\tau_0 + i(s_1 - s_4) \chi_{\eta_1 \eta_4}(s_1 - s_4)]^{2\nu} [\tau_0 + i(s_2 - s_3) \chi_{\eta_2 \eta_3}(s_2 - s_3)]^{2\nu}}, \tag{S10}
\end{aligned}$$

where terms in red highlight contributions from two extra non-equilibrium pairs, at moments s_3 and s_4 . The red term of the first line indicates the self-contraction of two extra anyonic pairs. The last two lines, on the other hand, refer to two possible extra phases, produced due to “braiding” between non-equilibrium operators and (i) the fermionic operators at the central QPC, or (ii) the other two anyonic operators (with labels 1 and 2) that participate Andreev-like tunneling. The phase from source (i) equals

$$\frac{[\tau_0 + i(t - s_3 - L) \chi_{-\eta_3}(t - s_3)] [\tau_0 + i(-s_4 - L) \chi_{+\eta_4}(-s_4)]}{[\tau_0 + i(t - s_4 - L) \chi_{-\eta_4}(t - s_4)] [\tau_0 + i(-s_3 - L) \chi_{+\eta_3}(-s_3)]} = \exp[i\pi(\eta_3 - \eta_4)] = 1, \tag{S11}$$

leading to a trivial result. This is a direct indicator that one electron (that tunnels at the central QPC) does not braid with an anyon. For case (ii), the phase equals

$$\frac{[\tau_0 + i(s_1 - s_3) \chi_{\eta_1 \eta_3}(s_1 - s_3)]^{2\nu} [\tau_0 + i(s_2 - s_4) \chi_{\eta_2 \eta_4}(s_2 - s_4)]^{2\nu}}{[\tau_0 + i(s_1 - s_4) \chi_{\eta_1 \eta_4}(s_1 - s_4)]^{2\nu} [\tau_0 + i(s_2 - s_3) \chi_{\eta_2 \eta_3}(s_2 - s_3)]^{2\nu}} = \exp[i\pi\nu(\eta_4 - \eta_3)], \tag{S12}$$

which is, in contrast to that of case (i), a non-trivial phase, as it involves ν . Here this phase factor comes from “braiding” between both source operators, and these in the middle arm. Following the analysis above, this phase is produced due to “braiding” between reflected anyonic holes and non-equilibrium anyons (with labels 3 and 4, of the case under consideration) that do not participate in Andreev-like tunneling. Notice that this phase factor actually equals the “braiding” phase in Refs. [S4, S5] for anyonic tunnelings at the central QPC. With these two phase factors, we can figure out the contribution of two extra non-equilibrium pairs, by integrating over s_1 and s_2 , leading

to

$$\sum_{\eta_3\eta_4} \eta_3\eta_4 \iint ds_3 ds_4 \frac{e^{-i\nu V(s_3-s_4)}}{[\tau_0 + i(s_3-s_4)\chi_{\eta_3\eta_4}(s_3-s_4)]^{2\nu}} \quad (\text{S13})$$

$$= t (1 - e^{2i\pi\nu}) 2 \sin(2\pi\nu) \Gamma(1 - 2\nu) (\nu V)^{2\nu-1}.$$

Combining all factors, we arrive at

$$D_{A2} = \frac{\tau_0^{\frac{1}{\nu}-1} c(\nu)}{2\pi(\tau_0 + it)^{1/\nu}} \frac{I_{A0}}{(\nu V)^{2\nu-1}} (it)^{2-2\nu} e^{i\nu V t} \left[-\frac{I_{A0}}{\nu} (1 - e^{2i\pi\nu}) t \right], \quad (\text{S14})$$

where the term in the square bracket has exactly the same form as that of the leading disconnected contribution of Ref. [S5]. We thus arrive at the conclusion that an extra pair of non-equilibrium anyons, introduced by the next-leading-order processes, induces a correction to the correlation function (of a connected diagram), due to “braiding” between this extra pair of non-equilibrium anyons and fractional-charge hole produced in the course of Andreev-like tunneling.

We can further extend the expansion of the correlation function to higher orders. By doing so, non-equilibrium anyons that do not Andreev-tunnel at the central QPC play the role of non-equilibrium anyons in Refs. [S5, S8]. A resummation is thus again valid for non-equilibrium anyons that correspond to disconnected diagrams. We can perform this resummation by, for instance, considering the expansion to the $2n$ th order in diluter transmissions. Note that at this stage, each expanded operator can either be a creation, or annihilation operator. Without loss of generality, we assume operators at moments s_1 and s_2 as connected ones, and for the rest of them, the $2i-1$ th operator (assumed as an annihilation operator) contracted with the $2i$ th one (assumed as a creation operator), with i an integer between 2 and n . For this option, the correlation becomes

$$\frac{\tau_0^{2\nu+1/\nu} [\tau_0 + i(t-s_1-L)\chi_{-\eta_1}(t-s_1)] [\tau_0 + i(-s_2-L)\chi_{+\eta_2}(-s_2)]}{(\tau_0 + it)^{1/\nu-1} [\tau_0 + i(s_1-s_2)\chi_{\eta_1\eta_2}(s_1-s_2)]^{2\nu-1} (\tau_0 + it) [\tau_0 + i(s_1-s_2)\chi_{\eta_1\eta_2}(s_1-s_2)]}$$

$$\times \frac{1}{[\tau_0 + i(t-s_2-L)\chi_{-\eta_2}(t-s_2)] [\tau_0 + i(-s_1-L)\chi_{+\eta_1}(-s_1)]}$$

$$\times \prod_{j=2}^n \iint ds_{2j-1} ds_{2j} \exp[i\pi\nu(\eta_{2j} - \eta_{2j-1})] \frac{\tau_0^{2\nu}}{[\tau_0 + i(s_{2j-1}-s_{2j})\chi_{\eta_{2j-1}\eta_{2j}}(s_{2j-1}-s_{2j})]^{2\nu}}, \quad (\text{S15})$$

where the first two lines are the leading-order result, with only connected-diagram contribution taken into consideration. The last line, on the other hand, refers to contribution with extra $n-1$ pairs of self-contracted non-equilibrium operators, where the “entanglement phase”, akin to Eqs. (S11) and (S12), has already been included. Notice that by doing so, corresponding contract option [as mentioned above Eq. (S15)] has been taken. Importantly, following Eq. (S15), with multiple (i.e., $n-1$) pairs of self-contracted operators, the contribution of these pairs [i.e., the last line of Eq. (S15)] simply equals the product of $n-1$ copies of the single-pair result. This fact is the prerequisite of resummation performed in e.g., Ref. [S5].

Now we consider the number of options. To start with, we have $2n(2n-1)$ ways to choose two operators (one creation and one annihilation) for a connected diagram. Next, we need to pair up the rest $2n-2$ non-equilibrium operators (disconnected contractions), with the number of options

$$\frac{2^{n-1}}{(n-1)!} C_{2n-2}^2 C_{2n-4}^2 \cdots C_2^2 = \frac{(2n-2)!}{(n-1)!}, \quad (\text{S16})$$

where the factor 2^{n-1} indicates that one can choose any operator of the chosen self-contracted pair to be the creation operator, while the factor $1/(n-1)!$ removes repeated options, as it does not make any difference to pick up one pair earlier or later. Now, restoring the prefactor $1/(2n!)$ from the expansion, the resummation becomes

$$\begin{aligned} \sum_{n=1}^{\infty} \left[-\frac{I_{A0}}{\nu} (1 - e^{2i\pi\nu}) t \right]^{n-1} \frac{(2n-2)!}{(n-1)!} (2n-1) 2n \frac{1}{(2n)!} &= \sum_{n=1}^{\infty} \frac{\left[-\frac{I_{A0}}{\nu} (1 - e^{2i\pi\nu}) t \right]^{n-1}}{(n-1)!} \\ &= \exp \left[-\frac{I_{A0}}{\nu} (1 - e^{2i\pi\nu}) t \right], \end{aligned} \quad (\text{S17})$$

which equals the exponential term of Eq. (8) of the main text, after taking $I_{A0} \rightarrow I_{A0}/e$, i.e., adding back constant factors. Finally, we arrive at correlation functions, after resummation over disconnected pairs

$$\sum_{n=0}^{\infty} D_{An} = \frac{\tau_0^{\frac{1}{\nu}-1}}{2\pi(a+it)^{1/\nu}} \left\{ 1 + e^{i\nu V t} c(\nu) \frac{it I_{A0}}{(i\nu V t)^{2\nu-1}} \exp \left[- (1 - e^{2i\pi\nu}) \frac{I_{A0} t}{\nu} \right] \right\}. \quad (\text{S18})$$

IC. Integral over time t

To obtain the expressions for the tunneling noises, Eqs. (2) and (3) of the main text, we need to perform an integration over time for correlation functions displayed in Eq. (8). It involves integral of the type

$$\int dt \frac{e^{-b|t|+ict}}{(\tau_0 + it)^{n_0}} \approx \frac{2b}{(n_0-2)(n_0-1)} \tau_0^{2-n_0} + \frac{4bc}{(n_0-3)(n_0-2)(n_0-1)} \tau_0^{3-n_0}, \quad (\text{S19})$$

where $b > 0$ and c are both real numbers and we have expanded the result to the leading order in the ultraviolet cutoff τ_0 . For the cases we study, n_0 equals $\frac{2}{\nu} + 2\nu - 2$ for single-source contributions, and $\frac{2}{\nu} + 4\nu - 4$ for double-source ones. For Laughlin quasiparticles $\nu \leq 1/3$, $n_0 > 3$ is satisfied for both contributions. Following Eq. (S19), to the leading order in a , only the value of b matters. This fact indicates that, in contrast to the anyonic-tunneling case [S4, S5], for electronic tunnelings at the central QPC, the involved integrals are dominated by the ultraviolet limit, $t \rightarrow a$. Within our analysis of noise, b corresponds to non-equilibrium current: I_{A0} or I_{B0} for the single-source case, and $I_+ = I_{A0} + I_{B0}$ for the double-source case. The proportionality of the time integral to the non-equilibrium current indicates that

one cannot neglect disconnected diagrams (which produce the exponential suppression $\exp\{-[1 - \exp(\pm 2i\pi\nu)I_{A0,B0}/\nu e]t\}$) when calculating noise or current, in systems with Andreev-like tunneling.

We are now ready to calculate tunneling current and tunneling current noise, which involve the integral of correlation functions

$$\begin{aligned} S_T &= v_F^2 e^3 T_C \int dt \left\langle \left\{ \Psi_B^\dagger(0) \Psi_A(0), \Psi_A^\dagger(t) \Psi_B(t) \right\} \right\rangle_{T_C=0}, \\ I_T &= e^2 v_F^2 T_C \int dt \left\langle \left[\Psi_B^\dagger(0) \Psi_A(0), \Psi_A^\dagger(t) \Psi_B(t) \right] \right\rangle_{T_C=0}, \end{aligned} \quad (\text{S20})$$

where v_F is the Fermi velocity. Integrals of Eq. (S20) can be evaluated with Eqs. (S19) and (S18), leading to explicit expressions (assuming $V_{sA} = V_{sB} = V$)

$$\begin{aligned} I_T(T_A, 0) &= -T_C \frac{T_A}{\pi^2} \frac{2 \left[\frac{I_{A0}}{\nu} (1 - \cos 2\pi\nu) \right] \left[\frac{e}{\hbar} \nu V + \frac{I_{A0}}{e\nu} \sin 2\pi\nu \right]}{\left(\frac{2}{\nu} + 2\nu - 3 \right) \left(\frac{2}{\nu} + 2\nu - 4 \right) \left(\frac{2}{\nu} + 2\nu - 5 \right)} \tau_0, \\ I_T(0, T_B) &= T_C \frac{T_B}{\pi^2} \frac{2 \left[\frac{I_{B0}}{\nu} (1 - \cos 2\pi\nu) \right] \left[\frac{e}{\hbar} \nu V + \frac{I_{B0}}{e\nu} \sin 2\pi\nu \right]}{\left(\frac{2}{\nu} + 2\nu - 3 \right) \left(\frac{2}{\nu} + 2\nu - 4 \right) \left(\frac{2}{\nu} + 2\nu - 5 \right)} \tau_0, \\ I_T(T_A, T_B) &= -T_C \frac{T_A T_B}{\pi^2} \frac{8 \sin^3 \pi\nu \cos \pi\nu \frac{I_+ I_-}{e\nu^2}}{\left(\frac{2}{\nu} + 4\nu - 5 \right) \left(\frac{2}{\nu} + 4\nu - 6 \right) \left(\frac{2}{\nu} + 4\nu - 7 \right)} \tau_0, \\ S_T(T_A, 0) &= T_C \frac{T_A}{\pi^2} \frac{2\nu \sin^2(\pi\nu) e I_{A0}}{(2 - 3\nu + 2\nu^2)(2 - 4\nu + 2\nu^2)}, \\ S_T(0, T_B) &= T_C \frac{T_B}{\pi^2} \frac{2\nu \sin^2(\pi\nu) e I_{B0}}{(2 - 3\nu + 2\nu^2)(2 - 4\nu + 2\nu^2)}, \\ S_T(T_A, T_B) &= T_C \frac{T_A}{\pi^2} \frac{2\nu \sin^2(\pi\nu) e I_{A0}}{(2 - 3\nu + 2\nu^2)(2 - 4\nu + 2\nu^2)} + T_C \frac{T_B}{\pi^2} \frac{2\nu \sin^2(\pi\nu) e I_{B0}}{(2 - 3\nu + 2\nu^2)(2 - 4\nu + 2\nu^2)} \\ &\quad + T_C \frac{T_A T_B}{\pi^2} \frac{2\nu \sin^2(\pi\nu) e (I_{A0} + I_{B0})}{(2 - 5\nu + 4\nu^2)(2 - 6\nu + 4\nu^2)}, \end{aligned} \quad (\text{S21})$$

which, in comparison to the noise, are proportional to the ultraviolet cutoff τ_0 .

II. Finite-temperature expressions

In the main text, we assume that both sources are fixed by the voltage bias V , with respect to two middle edges A and B . With this assumption, single-source measurement can be obtained by pinching off one of two diluters, which tunes either T_A or T_B to be zero.

In real experiments, the single-source correlation measurement can be alternatively performed by turning off either source, i.e., keeping the corresponding source grounded. This option (i.e., taking zero voltage bias) is, however, ill-captured by Eq. (8), because of the divergence of Eq. (10) in the $V \rightarrow 0$ limit. Indeed, when $V \rightarrow 0$, a finite temperature must be assumed, to avoid the current divergence, and keep the diluter in the anyonic tunneling limit. In this section, we thus take a finite temperature T . We

assume that (i) T is much smaller than the corresponding bias, if the source is on, and (ii) T is also large enough to keep the diluter in the anyonic tunneling limit, in which anyons are allowed to tunnel through the diluting QPC. Notice that a finite temperature, or even the temperature difference, is capable of disclosing anyonic statistical feature [S9], due to the connection between delta-T noise (noise induced by a temperature difference) and operator scaling dimension [S10–S12], which is proportional to the filling factor.

IIA. Modifications on the non-equilibrium current

The inclusion of a finite temperature introduces two modifications: a modification of the non-equilibrium current through diluters and the modification of contour integrals. At finite temperatures, the non-equilibrium current through a diluter involves the following integral:

$$\int dt \frac{(\pi k_B T)^{2\nu} e^{i\frac{\nu e V}{\hbar} t}}{\sin^{2\nu}[\pi k_B T(\tau_0 + it)/\hbar]} = (2\pi k_B T)^{2\nu-1} \frac{\hbar}{2\pi\Gamma(2\nu)} e^{\frac{\nu e V}{4\pi k_B T}} \left| \Gamma\left(\nu + \frac{i\nu e V}{4\pi^2 k_B T}\right) \right|^2, \quad (\text{S22})$$

where $2\nu < 1$ is assumed, as in the main text. This integral, which refers to the current from one source, was addressed, in particular, in Ref. [S13]. With this integral, the leading-order currents that enter the two middle edges become

$$I_{A0,B0}(V_{sA,sB}, T) = \frac{e^2}{\tau_0} \frac{T_{A,B}}{4\pi^2} \left(\frac{2\pi k_B T \tau_0}{\hbar} \right)^{2\nu-1} \times \frac{\nu}{\pi\Gamma(2\nu)} \sinh\left(\frac{\nu e V_{sA,sB}}{2k_B T}\right) \left| \Gamma\left(\nu + \frac{i\nu e V_{sA,sB}}{2\pi k_B T}\right) \right|^2, \quad (\text{S23})$$

where V_{sA} and V_{sB} refer to the bias in sources sA and sB , respectively. We can briefly capture the current features by checking the asymptotic scaling of the function that depends on $\nu e V_{sA,sB}/k_B T$, i.e.,

$$\sinh(x) \left| \Gamma(\nu + ix/\pi) \right|^2 \propto \begin{cases} x, & \text{if } x \ll 1, \\ x^{2\nu-1}, & \text{if } x \gg 1. \end{cases} \quad (\text{S24})$$

Following the asymptotic features above,

$$I_{A0,B0} \propto T_{A,B} (eV_{sA,sB})^{2\nu-1}$$

for $\nu V_{sA,sB} \gg 2T$, in agreement with Eqs. (9) and (10) of the main text. In the opposite limit $\nu e V_{sA,sB} \ll 2k_B T$, we get

$$I_{A0,B0} \propto T_{A,B} (k_B T)^{2\nu-2} eV_{sA,sB}.$$

In both limits, the current equals the product of $eV_{sA,sB}$, and the renormalization factor $[\max(\nu eV_{sA,sB}, 2k_B T)]^{2\nu-2}$, in agreement with the scaling analysis for anyonic tunneling through a QPC.

IIB. Finite-temperature contour integral

The introduction also modifies the contour integral. In this section, we focus, without loss of generality, on subsystem \mathcal{A} . **We once again take $e = \hbar = v_F = 1$ in this subsection, to simplify the derivation. These constant factors will be included when showing the final results.** The finite-temperature situation involves two integrals below

$$\begin{aligned} & \int ds_1 \frac{e^{-i\nu V_{sA} s_1}}{\sinh\{\pi T[i\tau_0\chi + \eta_1(-s_1) - (-s_1 - L)]\}} \int ds_2 \frac{e^{i\nu V_{sA} s_2}}{\sinh\{\pi T[i\tau_0\chi - \eta_2(t - s_2) - (t - s_2 - L)]\}} \\ &= \int ds_1 \frac{e^{i\nu V_{sA} s_1}}{\sinh[\pi T(s_1 - i\tau_0\eta_1)]} \int ds_2 \frac{e^{-i\nu V_{sA} s_2}}{\sinh[\pi T(s_2 - i\tau_0\eta_2)]}, \end{aligned} \tag{S25}$$

where we have shifted $s_1 \rightarrow -s_1 - L$, $s_2 \rightarrow -s_2 + t - L$, and taken the large- L limit for the second line. These integrals contain poles at $s_1 = i\tau_0\eta_1 + n_1/T$ and $s_2 = i\tau_0\eta_2 + n_2/T$, where n_1 and n_2 are integers, with their value ranges determined by η_1 and η_2 . Indeed, since $V_A > 0$, integrals over s_1 and s_2 include the upper and lower half-planes, respectively. As a consequence, $n_1 \geq 0$ if $\eta_1 = 1$, and $n_1 \geq 1$ otherwise; $n_2 \leq 0$ if $\eta_2 = -1$, and $n_2 \leq -1$ otherwise. In contrast to the zero-temperature case, now η_1 and η_2 can take both values, as thermal fluctuations allow (exponentially suppressed) tunneling from A to sA .

Since poles of s_1 and s_2 contain integer factors, the contour integrals will be expressed in terms of series over n_1 and n_2 . Now, the correlator D_{A1} is evaluated as

$$\begin{aligned}
D_{A1} &= -\frac{T_A}{(2\pi\tau_0)^3} \iint \frac{ds_1 ds_2 \sum_{\eta_1 \eta_2} \eta_1 \eta_2 (\pi T \tau_0)^{\frac{1}{\nu}+2\nu} e^{-i\nu V_{sA}(s_1-s_2)}}{\sin^{1/\nu}[\pi T(\tau_0+it)] \sin^{2\nu} \{2\pi^2 T[\tau_0+i(s_1-s_2)\chi_{\eta_1 \eta_2}(s_1-s_2)]\}} \\
&\times \frac{\sin \{ \pi T[\tau_0+i(t-s_1-L)\chi_{-\eta_1}(t-s_1)] \} \sin \{ \pi T[\tau_0+i(-s_2-L)\chi_{+\eta_2}(-s_2)] \}}{\sin \{ \pi T[\tau_0+i(t-s_2-L)\chi_{-\eta_2}(t-s_2)] \} \sin \{ \pi T[\tau_0+i(-s_1-L)\chi_{+\eta_1}(-s_1)] \}} \\
&= \frac{T_A}{(2\pi\tau_0)^3} \sum_{\eta_1 \eta_2} \eta_1 \eta_2 \frac{(\pi T \tau_0)^{\frac{1}{\nu}+2\nu}}{\sin^{\frac{1}{\nu}-1}[\pi T(\tau_0+it)]} e^{i\nu V_{sA} t} \\
&\times \iint ds_1 ds_2 \frac{\chi_{\eta_1 \eta_2}(s_2-s_1-t) \sin^{1-2\nu} \{ \pi T(\tau_0+i(s_2-s_1-t)\chi_{\eta_1 \eta_2}(s_2-s_1-t) \}}{e^{-i\nu V_{sA}(s_1-s_2)} \sinh[\pi T(s_1-i\tau_0\eta_1)] \sinh[\pi T(s_2-i\tau_0\eta_2)]} \\
&= \frac{T_A}{(2\pi\tau_0)^3} \sum_{\eta_1 \eta_2} \eta_1 \eta_2 \frac{(\pi T \tau_0)^{\frac{1}{\nu}+2\nu}}{\sin^{\frac{1}{\nu}-1}[\pi T(\tau_0+it)]} e^{i\nu V_{sA} t} \frac{4\pi^2}{(\pi T)^2} (-\eta_1) \sin^{1-2\nu}(i\pi T t \eta_1) \\
&\times \sum_{n_1=(1-\eta_1)/2}^{\infty} \sum_{n_2=(1+\eta_2)/2}^{\infty} e^{-\frac{\nu V_{sA}}{T} n_1} e^{-\frac{\nu V_{sA}}{T} n_2} \theta^{1-2\nu}(n_1+n_2) \\
&= \frac{T_A}{2\pi\tau_0} \frac{(\pi T \tau_0)^{\frac{1}{\nu}+2\nu-2}}{\sin^{\frac{1}{\nu}+2\nu-2}[\pi T(\tau_0+it)]} e^{i\nu V_{sA} t} \frac{[1-\exp(-\frac{\nu V_{sA}}{T})] [1-(-1)^{-2\nu} \exp(-\frac{\nu V_{sA}}{T})]}{1+\exp(-\frac{2\nu V_{sA}}{T})}, \tag{S26}
\end{aligned}$$

where $\theta(n) = 1$ if n is even, and equals -1 if n becomes odd. Equation (S26) transforms into the zero-temperature expression when $V_{sA} \gg T$, and becomes proportional to V_{sA}/T in the opposite limit. This fact, in combination with Eq. (S23) for the non-equilibrium current, indicates that in the $V_{sA} \ll T$ limit (i.e., when source sA turned-off), one should replace $I_{A0,B0}/(\nu V_{sA,sB})^{2\nu-1}$ of Eqs. (8)-(10) of the main text, by the modified expression $I_{A0,B0}/(2\pi T)^{2\nu-1}$.

Based on the expressions above, we conclude that one can obtain the single-source contribution by tuning one of the source voltage biases (V_{sA} or V_{sB}) to zero. It is equivalent to pinching off the corresponding diluter (i.e., setting T_A or T_B to zero), as suggested in Eqs. (2) and (3) in the main text.

Finally, to end this section, we, as promised, present the result after adding back all constant factors, leading to

$$\begin{aligned}
D_{A1} &= \frac{T_A}{2\pi\tau_0} v_F^2 \frac{(\pi k_B T \tau_0 / \hbar)^{\frac{1}{\nu}+2\nu-2}}{\sin^{\frac{1}{\nu}+2\nu-2}[\pi k_B T(\tau_c+it)/\hbar]} e^{i\nu e V_{sA} t / \hbar} \\
&\times \frac{[1-\exp(-\frac{\nu e V_{sA}}{k_B T})] [1-(-1)^{-2\nu} \exp(-\frac{\nu e V_{sA}}{k_B T})]}{1+\exp(-\frac{2\nu e V_{sA}}{k_B T})}. \tag{S27}
\end{aligned}$$

III. Modifications from interactions

In the main text, we comment that the entanglement pointer $\mathcal{P}_{\text{Andreev}}$ has a stronger resilience (than that of the tunneling-current noise) against interaction effects. In this section, we demonstrate this by including the screened Coulomb interaction that couples the charge density in edge A with the charge density in edge B . **We once again take $v_F = \hbar = e = 1$ during derivations. These constant factors will be re-introduced when showing the final results.**

III.A. Interaction's effect on correlation functions

In this section, we consider the model of Fig. S1, where we introduce Coulomb interaction between edges A and B only in the shadowed area (i.e., $-d \leq x \leq d$ in Fig. S1, with $d < L$). For simplicity, we further assume a constant interaction (quantified by the Luttinger liquid parameter K) within the interacting area (in the experiment, this would correspond to the effect of screening of the long-range Coulomb repulsion by gates).

It is worth noting that in this section, we are choosing a different convention of spatial coordinates: now the two diluters are placed at $x = \pm L$, and the central QPC is located at $x = 0$. Indeed, (formally) non-local interactions would be introduced, if staying with the convention of other sections (i.e., in the way that x increases along corresponding downstream directions of each edge).

Within the interacting area, Luttinger-type interactions are easily incorporated within the bosonization approach. For our later convenience, we follow Ref. [S14], and use canonical fields to bosonize fermionic operators Ψ_A and Ψ_B ,

$$\Psi_A(x) = \frac{F_A}{\sqrt{2\pi a}} e^{ik_F x} e^{i[\theta(x) - \phi(x)]}, \quad \Psi_B(x) = \frac{F_B}{\sqrt{2\pi a}} e^{-ik_F x} e^{i[\theta(x) + \phi(x)]}, \quad (\text{S28})$$

where canonical phases follow the standard commutator $[\phi(x), \theta(x')] = i\pi\delta(x' - x)$, and are related to our original fields following $\phi_A = \theta - \phi$ and $\phi_B = \theta + \phi$. Without interaction, ϕ_A and ϕ_B are the right-going and left-going modes in edges A and B , respectively. However, they are no longer chiral modes in the interacting area. Indeed, now the left-going and right-going chiral modes become $\phi_{\pm} = K\theta \mp \phi$, where K refers to the Luttinger liquid parameter. In the interacting area, edge fields and chiral fields are connected via

$$\begin{aligned} \phi_A(x) &= \phi_+(x) + \left(\frac{1}{2K} - \frac{1}{2}\right) [\phi_+(x) + \phi_-(x)], \\ \phi_B(x) &= \phi_-(x) + \left(\frac{1}{2K} - \frac{1}{2}\right) [\phi_+(x) + \phi_-(x)]. \end{aligned} \quad (\text{S29})$$

For later convenience, we further define

$$\delta_{\text{edge}} \equiv \frac{1}{2K} - \frac{1}{2}, \quad (\text{S30})$$

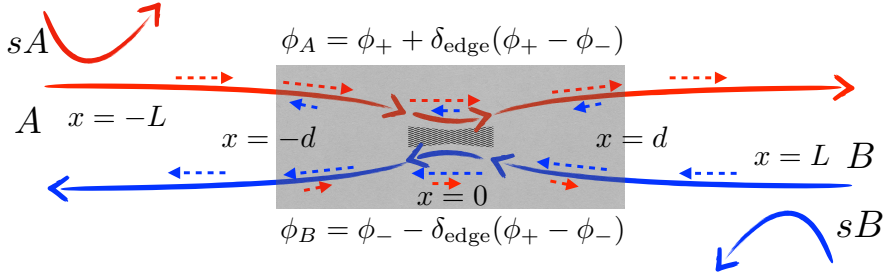


Fig. S1 The schematics of the model with interaction between the two edges. We choose the convention of spatial coordinate such that x increases from left to right. Two diluters and the central QPC are placed at $x = \pm L$ and $x = 0$, respectively. Within the area $-d \leq x \leq d$ (indicated by the shaded gray box), particles in edge A interact with particles in edge B , with the interaction strength quantified by the Luttinger parameter K . Outside the interacting area, the bosonic fields ϕ_A and ϕ_B equal the right-going and left-going chiral fields ϕ_+ (the red dashed arrow) and ϕ_- (the blue dashed arrow), respectively. Within the interacting area, ϕ_A and ϕ_B are linear combinations of ϕ_+ and ϕ_- .

as the parameter that quantifies the effective difference from a non-interacting situation. In addition to Eq. (S29) for the rotation of fields, interaction also modifies the quasiparticle velocity. Indeed, following Ref. [S14], within the interacting area, the velocity u and the Luttinger liquid parameter K are related to the inter-edge interaction, following (after taking $v_F = 1$)

$$u = \sqrt{1 - (g_2/2)^2}, \quad K = \sqrt{\frac{1 - g_2/2}{1 + g_2/2}}, \quad (\text{S31})$$

where g_2 refers to the strength of the inter-edge Coulomb interaction (interaction between counterpropagating bare modes). We can then express the “plasmon” velocity in the interacting area in terms of K ,

$$u = \frac{2K}{1 + K^2} \approx 1 - \frac{(K - 1)^2}{2}, \quad (\text{S32})$$

where we have taken the weak-interaction assumption ($|K - 1| \ll 1$) to expand u to leading order in interaction. In comparison to $\delta_{\text{edge}} \approx (1 - K)/2$ that is linear to $(1 - K)$, the leading interaction-induced modification of the velocity is quadratic in $(1 - K)$, underscoring a comparatively smaller correction from weak interactions. In this section, we thus approximately take $u = 1$ in our calculation.

As we introduce sharp boundaries $x = \pm d$ that abruptly separate interacting and non-interacting areas, boundary conditions should be installed at these two boundaries. These boundary conditions describe the Fresnel scattering of bosonic modes at the interfaces separating two media with different “optical” properties. This type scattering gives rise to fractionalization of the charge excitations at the interfaces [S15–S18].

Briefly, since edges A and B are spatially separated, we can enforce current conservation in each edge separately, at different boundaries. For the boundary at $x = -d$,

the incoming current in edge A equals $\partial_x \phi_A / (2\pi)$. This current should be equal to the current in edge A , right into the interacting area. The current conservation requires the knowledge of current operators inside and outside of the interacting area. More specifically, outside the interacting area, $\phi_{A,B}(x, t) = \phi_{\pm}(x \mp t)$, meaning that the current operator

$$\hat{I}_{A,B}(|x| > d) = -\partial_t \phi_{\pm}(x \mp t) / 2\pi = \pm \partial_x \phi_{\pm} / 2\pi$$

(as a reminder, we take Fermi velocity $v_F = 1$ for simplicity in this work). Inside the interacting area, instead $\phi_{A,B}(x, t) = (1 + \delta_{\text{edge}})\phi_{\pm}(x \mp t) + \delta_{\text{edge}}\phi_{\mp}(x \pm t)$, leading to a modified current operator (we recall that we have neglected the difference of u from 1, which is quadratic in the interaction strength)

$$\begin{aligned} \hat{I}_{A,B}(|x| < d) &= -\frac{1 + \delta_{\text{edge}}}{2\pi} \partial_t \phi_{\pm}(x \mp t) - \frac{\delta_{\text{edge}}}{2\pi} \partial_t \phi_{\mp}(x \pm t) \\ &= \pm \frac{1 + \delta_{\text{edge}}}{2\pi} \partial_x \phi_{\pm}(x \mp t) \mp \frac{\delta_{\text{edge}}}{2\pi} \partial_x \phi_{\mp}(x \pm t). \end{aligned} \quad (\text{S33})$$

Current conservation then leads to the following relations between the phases at the interfaces:

$$\begin{aligned} \phi_A(-d^-) &= \phi_+(-d^+) + \delta_{\text{edge}}[\phi_+(-d^+) - \phi_-(-d^+)], \\ \phi_B(d^+) &= \phi_-(d^-) + \delta_{\text{edge}}[-\phi_+(d^-) + \phi_-(d^-)], \end{aligned} \quad (\text{S34})$$

where superscript \pm in d^{\pm} labels the right and left sides, respectively, of a given boundary. Since $\phi_{A,B}$ are free chiral fields in the non-interacting regions, with expressions of Eq. (S34), one can keep track of the positions of ϕ_{\pm} fields at earlier time moments, to express fields at diluters as

$$\begin{aligned} \phi_A(-L, s) &= \phi_A(-d, s + L - d) = (1 + \delta_{\text{edge}})\phi_+(-d, s + L - d) - \delta_{\text{edge}}\phi_-(-d, s + L - d), \\ \phi_B(L, s) &= \phi_B(d, s + L - d) = (1 + \delta_{\text{edge}})\phi_-(d, s + L - d) - \delta_{\text{edge}}\phi_+(d, s + L - d). \end{aligned} \quad (\text{S35})$$

For further convenience, it is useful to imagine an auxiliary wire where the interaction region would be extended to the positions of diluters. In the interacting part of our setup, $|x| < d$, the chiral fields are equivalent to those in the auxiliary one: $\phi_{\pm}(x, t) = \tilde{\phi}_{\pm}(x, t)$. In the auxiliary system, we can further use $\tilde{\phi}_+(-d, s + L - d) = \tilde{\phi}_+(L, s)$ and $\tilde{\phi}_-(-d, s + L - d) = \tilde{\phi}_-(-2d + L, s)$. Thus, the fields $\phi_{A,B}(-L, s)$ in the noninteracting parts of our setup near the diluters can be replaced by the combinations of the chiral fields $\tilde{\phi}_{\pm}$ of the virtual wire, where interaction is everywhere:

$$\phi_A(-L, s) \rightarrow (1 + \delta_{\text{edge}})\tilde{\phi}_+(-L, s) - \delta_{\text{edge}}\tilde{\phi}_-(-2d + L, s), \quad (\text{S36})$$

$$\phi_B(L, s) \rightarrow (1 + \delta_{\text{edge}})\tilde{\phi}_-(L, s) - \delta_{\text{edge}}\tilde{\phi}_+(2d - L, s). \quad (\text{S37})$$

Equations (S35) indicate that although field operators at two diluters are non-interacting, they can be written in terms of two counter-propagating fields of the auxiliary wire. This substitution of fields is taken since ϕ_A and ϕ_B are not independent fields at the central QPC [see Eq. (S38) below]. In what follows, for brevity, we will remove the tildes from fields in the virtual wire.

With these expressions, we are ready to analyze the correlation function, in the presence of interaction. To begin with, after including interactions, the correlator at the central QPC becomes

$$\begin{aligned}
& T_C \langle T_K \Psi_A^\dagger(0, t^-) \Psi_B(0, t^-) \Psi_B^\dagger(0, 0^+) \Psi_A(0, 0^+) \rangle \\
&= \frac{T_C}{(2\pi a)^2} \left\langle T_K e^{-i\frac{1}{\sqrt{\nu}}[\phi_A(0, t^-) - \phi_B(0, t^-)]} e^{i\frac{1}{\sqrt{\nu}}[\phi_A(0, 0^+) - \phi_B(0, 0^+)]} \right\rangle \\
&= \frac{T_C}{(2\pi a)^2} \left\langle T_K e^{-i\frac{1}{\sqrt{\nu}}\phi_+(0, t^-)} e^{i\frac{1}{\sqrt{\nu}}\phi_+(0, 0^+)} \right\rangle \left\langle T_K e^{i\frac{1}{\sqrt{\nu}}\phi_-(0, t^-)} e^{-i\frac{1}{\sqrt{\nu}}\phi_-(0, 0^+)} \right\rangle,
\end{aligned} \tag{S38}$$

where now we need to evaluate the correlation function for \pm modes, instead of A and B modes. As a reminder, Eq. (S38) can not capture the situation where edges A and B are biased at different voltages, as this situation requires the inclusion of another voltage-difference-dependent (and time-dependent) phase factor: in this non-equilibrium case the \pm modes are not at equilibrium. However, we can still use Eq. (S38) for calculating perturbative expansions in diluter's transmissions even in the single-source case, since all the involved averages will be taken with respect to the equilibrium state.

As a direct consequence of interaction between the edges, now we cannot evaluate the correlation function of each subsystem (\mathcal{A} and \mathcal{B}) separately. For instance, when considering leading-order expansion at the upper diluter, the modified D_{A2} of Eq. (S9) contains correlations like [following $\phi_A - \phi_B = \phi_+ - \phi_-$, as given by Eq. (S38)]:

$$\begin{aligned}
& \sum_{\eta_1 \eta_2} \eta_1 \eta_2 \iint ds_1 ds_2 \left\langle e^{-i\sqrt{\nu}\phi_{sA}(-L, s_1^{\eta_1})} e^{i\sqrt{\nu}\phi_{sA}(-L, s_2^{\eta_2})} \right\rangle e^{i\nu V(s_1 - s_2)} \\
& \times \left\langle T_K e^{-i\frac{\phi_+(0, t^-)}{\sqrt{\nu}}} e^{i\frac{\phi_+(0, 0^+)}{\sqrt{\nu}}} e^{i\frac{\phi_-(0, t^-)}{\sqrt{\nu}}} e^{-i\frac{\phi_-(0, 0^+)}{\sqrt{\nu}}} e^{i\sqrt{\nu}\phi_A(-L, s_1^{\eta_1})} e^{-i\sqrt{\nu}\phi_A(-L, s_2^{\eta_2})} \right\rangle \\
&= \sum_{\eta_1 \eta_2} \eta_1 \eta_2 \iint ds_1 ds_2 \frac{\tau_0^\nu e^{i\nu V(s_1 - s_2)}}{[\tau_0 + i(s_1 - s_2)\chi_{\eta_1 \eta_2}(s_1 - s_2)]^\nu} \\
& \times \left\langle T_K e^{-i\frac{1}{\sqrt{\nu}}\phi_+(0, t^-)} e^{i\frac{1}{\sqrt{\nu}}\phi_+(0, 0^+)} e^{i\sqrt{\nu}(1 + \delta_{\text{edge}})\phi_+(-L, s_1^{\eta_1})} e^{-i\sqrt{\nu}(1 + \delta_{\text{edge}})\phi_+(-L, s_2^{\eta_2})} \right\rangle \\
& \times \left\langle T_K e^{i\frac{\phi_-(0, t^-)}{\sqrt{\nu}}} e^{-i\frac{\phi_-(0, 0^+)}{\sqrt{\nu}}} e^{-i\sqrt{\nu}\delta_{\text{edge}}\phi_-(-L - 2d, s_1^{\eta_1})} e^{i\sqrt{\nu}\delta_{\text{edge}}\phi_-(-L - 2d, s_2^{\eta_2})} \right\rangle \\
&= \sum_{\eta_1 \eta_2} \eta_1 \eta_2 \iint ds_1 ds_2 \frac{e^{i\nu V(s_1 - s_2)} \tau_0^{\frac{1}{2\nu} + 2\tilde{\nu}}}{(\tau_0 + it)^{\frac{1}{2\nu}} [\tau_0 + i(s_1 - s_2)\chi_{\eta_1 \eta_2}(s_1 - s_2)]^{2\tilde{\nu}}} \\
& \times \left\{ \frac{[\tau_0 + i(t - s_2 - L + 2d)\chi_{-\eta_2}(t - s_2)][\tau_0 + i(-s_1 - L + 2d)\chi_{+\eta_1}(-s_1)]}{[\tau_0 + i(t - s_1 - L + 2d)\chi_{-\eta_1}(t - s_1)][\tau_0 + i(-s_2 - L + 2d)\chi_{+\eta_2}(-s_2)]} \right\}^{\delta_{\text{edge}}} \\
& \times \left\{ \frac{[\tau_0 + i(t - s_2 - L)\chi_{-\eta_2}(t - s_2)][\tau_0 + i(-s_1 - L)\chi_{+\eta_1}(-s_1)]}{[\tau_0 + i(t - s_1 - L)\chi_{-\eta_1}(t - s_1)][\tau_0 + i(-s_2 - L)\chi_{+\eta_2}(-s_2)]} \right\}^{\frac{\tilde{\nu}}{\nu}},
\end{aligned} \tag{S39}$$

where $\tilde{\nu} \equiv \nu(1 + \delta_{\text{edge}})$ is influenced by interaction. Notice that bosonic operators with different chirality have different correlations: $\langle \phi_\pm(x, t)\phi_\pm(x', t') \rangle \propto \ln[(t \mp x) - (t' \mp x')]$.

The last line of Eq. (S39) refers to the Coulomb-interaction-influenced “tangling” of the right-going field ϕ_+ . It reduces to the last line of Eq. (S1) for the non-interacting case, after taking $\delta_{\text{edge}} = 0$. The last but one line instead refers to the field from the left-going field ϕ_- . This term is fully interaction-induced, as ϕ_- and ϕ_A are uncorrelated for the non-interacting situation.

We proceed by taking $s_1 \rightarrow s_2$ in equation above, to visit the disconnected diagram. We also perform shifts in time $s_1 \rightarrow s_1 - L$ and $s_2 \rightarrow s_2 - L$, with which the last two lines of Eq. (S39) equal

$$\left\{ \frac{[\tau_0 + i(t - s_1 + 2d)\eta_2][\tau_0 + i(-s_1 + 2d)\eta_1]}{[\tau_0 + i(t - s_1 + 2d)\eta_1][\tau_0 + i(-s_2 + 2d)\eta_2]} \right\}^{\delta_{\text{edge}}} \left\{ \frac{[\tau_0 + i(t - s_1)\eta_2][\tau_0 + i(-s_1)\eta_1]}{[\tau_0 + i(t - s_1)\eta_1][\tau_0 + i(-s_1)\eta_2]} \right\}^{\frac{\tilde{\nu}}{\nu}}. \quad (\text{S40})$$

The second part of Eq. (S40), which corresponds to the so-called “braiding” between right-going non-equilibrium anyons and ϕ_+ mode at the central QPC, equals $\exp[i\pi(\eta_2 - \eta_1)\tilde{\nu}/\nu]$. In contrast to the non-interacting result, this phase is non-trivial, and will not vanish after summations over Keldysh indexes. The first term of Eq. (S40) instead indicates the “braiding” between the ϕ_- mode at the central QPC, and counter-propagating non-equilibrium anyonic mode in the interacting area. In this section, we assume the large- d situation ($d > t$), with which this extra term equals one, a trivial value. Notice that for a small value of d (more specifically, when $2d < s_1, s_2 < t$), this term equals $\exp[i\pi\delta_{\text{edge}}(\eta_2 - \eta_1)]$. Combining this factor with the previous one (i.e., $\exp[i\pi(1 + \delta_{\text{edge}})(\eta_2 - \eta_1)]$), the total “tangling” part equals $\exp[i\pi(1 + 2\delta_{\text{edge}})(\eta_2 - \eta_1)]$ when considering disconnected diagrams, leading to an even stronger modification from interactions.

As another important piece of message, Eq. (S40) indicates that, when considering disconnected diagrams in the large- d assumption, interactions mainly influence the correlation between ϕ_A at the diluter and ϕ_+ at the central QPC. The $\phi_A - \phi_-$ correlation instead remains negligible even with interaction involved. Similarly, even for the interacting situation, we only need to worry about the correlation between ϕ_B at the diluter and ϕ_- at the central QPC.

In addition to disconnected diagrams, the interaction between edges A and B also influences the connected contraction. Briefly, by choosing the connected contraction (i.e., $s_1 \rightarrow t - L$ and $s_2 \rightarrow -L$), integrals over s_1 and s_2 of Eq. (S39) can be rewritten

as

$$\begin{aligned}
\text{(S39)} &= \frac{\tau_0^{\frac{1}{2\nu}+2\tilde{\nu}}}{(\tau_0+it)^{\frac{1}{2\tilde{\nu}}}} \sum_{\eta_1\eta_2} \eta_1\eta_2 \frac{(\tau_0+it\eta_2)^{\frac{\tilde{\nu}}{\nu}} [\tau_0+i(-t)\eta_1]^{\frac{\tilde{\nu}}{\nu}}}{[\tau_0+it\chi_{\eta_1\eta_2}(t)]^{2\tilde{\nu}}} \\
&\times \left\{ \frac{[\tau_0+i(t+2d)\eta_2][\tau_0+i(-t+2d)\eta_1]}{(\tau_0+i2d\eta_1)(\tau_0+i2d\eta_2)} \right\}^{\delta_{\text{edge}}} \\
&\times \iint ds_1 ds_2 \frac{e^{i\nu V(s_1-s_2)}}{\{[\tau_0+i(t-s_1-L)\chi_{-\eta_1}(t-s_1)][\tau_0+i(-s_2-L)\chi_{+\eta_2}(-s_2)]\}^{\frac{\tilde{\nu}}{\nu}}} \\
&= I_{\tilde{\nu}=\nu} \times \frac{(it/\tau_0)^{(2-2\nu)\frac{\tilde{\nu}}{\nu}}}{\Gamma^2\left(\frac{\tilde{\nu}}{\nu}\right)}, \tag{S41}
\end{aligned}$$

where $I_{\tilde{\nu}=\nu}$ refers to the non-interacting result, where $\tilde{\nu} = \nu$. The factor multiplying $I_{\tilde{\nu}=\nu}$ describes the modification from interactions.

With both modifications induced by the interaction taken into consideration, we arrive at modified correlation functions (notice, importantly, that the suppressing factor of the connected part is also influenced by interactions)

$$\begin{aligned}
\langle \Psi_+^\dagger(t^-)\Psi_+(0^+) \rangle &= \frac{\tau_0^{\frac{1}{\nu}-1}}{2\pi(\tau_0+it)^{\frac{1}{\nu}}} \left\{ e^{-(1-e^{2i\pi\frac{\tilde{\nu}}{\nu}})\frac{I_{A0}t}{e\nu}} \right. \\
&\quad \left. + \frac{c(\nu)(it/\tau_0)^{(2-2\nu)\frac{\tilde{\nu}}{\nu}}}{\Gamma^2\left(\frac{\tilde{\nu}}{\nu}\right)} \frac{it\frac{I_{A0}}{e}e^{i\nu eVt/\hbar}}{(i\nu eVt/\hbar)^{2\nu-1}} e^{-(1-e^{2i\pi\tilde{\nu}})\frac{I_{A0}t}{e\nu}} \right\}, \tag{S42} \\
\langle \Psi_-(t^-)\Psi_-^\dagger(0^+) \rangle &= \frac{\tau_0^{\frac{1}{\nu}-1}}{2\pi(\tau_0+it)^{\frac{1}{\nu}}} \left\{ e^{-(1-e^{-2i\pi\frac{\tilde{\nu}}{\nu}})\frac{I_{B0}t}{\nu}} \right. \\
&\quad \left. + \frac{c(\nu)(it/\tau_0)^{(2-2\nu)\frac{\tilde{\nu}}{\nu}}}{\Gamma^2\left(\frac{\tilde{\nu}}{\nu}\right)} \frac{it\frac{I_{B0}}{e}e^{-i\nu eVt/\hbar}}{(i\nu eVt/\hbar)^{2\nu-1}} e^{-(1-e^{-2i\pi\tilde{\nu}})\frac{I_{B0}t}{e\nu}} \right\},
\end{aligned}$$

where the first term in each correlation function comes from interaction-induced disconnected diagrams. Notice that I_{A0} and I_{B0} are not influenced, as both diluters, where the non-equilibrium current values are emitted, are outside of the interacting area. In Eq. (S42), we have added back constant factors.

IIIB. Interaction effects on noise

With interaction-modified correlation functions, Eq. (S42), we are ready to calculate the tunneling-current noise in the presence of interactions. More explicitly, in the paragraphs below, we will show that in the strongly diluted limit, interaction-induced disconnected diagrams [i.e., those yielding the first terms of Eq. (S42)] have the chance to produce a dominant contribution. Indeed, by picking up the first terms in both

lines of Eq. (S42), we obtain the correction of the tunneling current noise

$$S_{\text{disconnected}}^{\text{int}} = T_C \frac{\tau_0^{\frac{2}{\nu}-2}}{4\pi^2} \int dt \frac{e^{-\left(1-e^{2i\pi\frac{\tilde{\nu}}{\nu}}\right)\frac{I_{A0}t}{e\nu} - \left(1-e^{-2i\pi\frac{\tilde{\nu}}{\nu}}\right)\frac{I_{B0}t}{e\nu}}}{(\tau_0 + it)^{2/\nu}} \quad (\text{S43})$$

$$\approx T_C \frac{1}{4\pi^2} \frac{2\nu^2 e I_+ [1 - \cos(2\pi\frac{\tilde{\nu}}{\nu})]}{(2-2\nu)(2-\nu)},$$

where $I_+ \equiv I_{A0} + I_{B0}$, and we keep only leading power of the ultraviolet cutoff a . A careful inspection of Eq. (S43) discloses two interesting features. As the first one, in contrast to Eqs. (2) and (3) of the main text, $S_{\text{disconnected}}^{\text{int}}$, which comes from the interaction-induced disconnected diagrams, does not explicitly depend on T_A and T_B (although implicitly it depends on these two quantities through I_+). This fact indicates that $S_{\text{disconnected}}^{\text{int}}$ can become much larger than the interaction-free results [i.e., terms in Eqs. (2) and (3) of the main text] in the strongly diluted limit.

With interaction involved, the original single-source and double-source tunneling current noises become

$$S_{1A,1B}^{\text{int}} = T_C \frac{T_{A,B}}{\pi^2 \Gamma^2\left(\frac{\tilde{\nu}}{\nu}\right)} \frac{\nu \{1 - \cos[2\pi\tilde{\nu}]\} e I_{A0,B0} + \nu [1 - \cos(2\pi\frac{\tilde{\nu}}{\nu})] e I_{B0,A0}}{(2-3\nu+2\tilde{\nu}\nu)(2-4\nu+2\tilde{\nu}\nu)}, \quad (\text{S44})$$

$$S_2^{\text{int}} = T_C \frac{T_A T_B}{\pi^2 \Gamma^2\left(\frac{\tilde{\nu}}{\nu}\right)} \frac{\nu [1 - \cos(2\pi\tilde{\nu})] e I_+}{(2-5\nu+4\tilde{\nu}\nu)(2-6\nu+4\tilde{\nu}\nu)}.$$

Equation (S44) also contains corrections from interactions, as indicated by its explicit dependence on $\tilde{\nu}$. The modification is proportional to the interaction parameter $\delta_{\text{edge}} = (\tilde{\nu} - \nu)/\nu$ in the weak-interacting limit. Since $S_{1A,1B}^{\text{int}} \propto T_{A,B}$, $S_2^{\text{int}} \propto T_A T_B$ are proportional to small tunneling probabilities, we clearly see that the interaction-induced disconnected diagrams can introduce a correction, $S_{\text{disconnected}}^{\text{int}}$, that prevails over other interaction effect, given large enough interaction or strong enough dilutions. Actually, the correction from disconnected diagrams can even become potentially comparable to interaction-free results.

As another feature of Eq. (S43), the contribution from the interaction-induced disconnected diagrams is proportional to the total non-equilibrium current $I_+ = I_{A0} + I_{B0}$, which is a sum of the partial contributions of the two edges (this separation into the parts associated with the two edges occurs in spite of the electrostatic between them). This proportionality, importantly, indicates that $S_{\text{disconnected}}^{\text{int}}$, which becomes dominant in the strongly diluted limit (as analyzed above), can be avoided by removing single-source tunneling noises from the double-source one. This removal of single-source contribution is indeed what is taken into account by the design of $\mathcal{P}_{\text{Andreev}}$, which gives rise to a strong resistance of $\mathcal{P}_{\text{Andreev}}$ against interactions. We emphasize that the proportionality of $S_{\text{disconnected}}^{\text{int}}$ to I_+ arises from the fast decay in time $2/\nu > 1$, in the integral of Eq. (S43). Indeed, for anyonic tunneling, $2\nu < 1$, the result of the integral instead contains an anomalous power of the non-equilibrium current [S5].

Before closing this section, we stress that $S_{1A,1B}^{\text{int}}$ contains a contribution $\propto T_{A,B} I_{B0,A0}$ that vanishes with either source off—the same as S_2 . Physically, this term

refers to the situation where a tunneling electron from edge A (or B) “braids” with non-equilibrium anyons in edge B (or A). When interaction is weak, this term leads to the interaction-induced correction $\propto T_{B,A}\delta_{\text{edge}}$. This fact indicates that our invented function $\mathcal{P}_{\text{Andreev}}$ is only weakly influenced by interactions, as long as $\delta_{\text{edge}} \ll T_{A,B}$, when the interaction-induced electron-anyon “braiding” is negligible.

IV. Single-particle and two-particle analysis

In the main text, we provide analysis on the tunneling current noise and cross correlation noise. In this section, we show details on how to arrive at Eq. (5) of the main text.

As is known (see e.g., Refs. [S19, S20]) single-particle and two-particle scattering pictures apply to the analysis of non-interacting fermionic and bosonic systems, where non-equilibrium particles participate in scatterings at the tunneling QPC. This tunneling of non-equilibrium particles at the QPC turns out to be crucial to the application of the scattering method. Indeed, in Refs. [S4, S5, S8] where non-equilibrium anyons do not tunnel at the central QPC, the obtained result fully disagrees with the scattering-theory-expression of Ref. [S21]. This inapplicability of scattering theory greatly reduces the transparency of anyonic scatterings. For the Andreev situation, luckily, the leading contribution once again involves tunnelings of non-equilibrium particles, thus enabling the application of scattering theory. Indeed, as a piece of evidence, now correlation functions Eq. (8) can be divided into the equilibrium and non-equilibrium contributions, which is impossible for Refs. [S4, S5, S8] that allow anyons to tunnel.

IVA. The tunneling current noise

We first look into the tunneling current noise. As the classical benchmark, we begin by considering the reducible tunneling current noise

$$\begin{aligned} \langle \hat{I}_{\text{T}}^2 \rangle_{\text{dist}} &= W_A(1 - W_B)W_C + W_B(1 - W_A)W_C + W_AW_B2W_C(1 - W_C) \\ &= (W_A + W_B)W_C - 2W_C^2W_AW_B, \end{aligned} \quad (\text{S45})$$

where \hat{I}_{T} is the operator for the tunneling current from A to B , “dist” is short for “distinguishable”, while W_A and W_B refer to the probability to have a non-equilibrium anyon from sources A and B , respectively. We notice that Eq. (S45) contains a term $W_C^2W_AW_B$ that is proportional to the two-particle scattering probability W_AW_B . This term however disappears in the irreducible correlation, after the removal of the current average product $\langle \hat{I}_{\text{T}} \rangle^2 = W_C^2(W_A - W_B)^2$. Indeed, now the irreducible correlation of the distinguishable case becomes

$$\langle \delta \hat{I}_{\text{T}}^2 \rangle_{\text{dist}} = (W_A + W_B)W_C - (W_A^2 + W_B^2)W_C^2, \quad (\text{S46})$$

where $\delta \hat{I}_{\text{T}} \equiv \hat{I}_{\text{T}} - \langle \hat{I}_{\text{T}} \rangle$ is tunneling current fluctuation operator. Here Eq. (S46) is irrelevant to the two-particle scattering probability $\propto W_AW_B$. More specifically, it

equals the summation of that of two independent single-particle tunneling processes: a solid benchmark for the missing of quantum statistics. This fact, importantly, indicates that one can observe the statistical message from bilinear terms $\propto W_A W_B$.

Now we move to consider indistinguishable particles. When two anyons arrive at the central QPC simultaneously, the chance to have an Andreev-like tunneling is modified, in comparison to the distinguishable case. For simplicity, we call the chance to have the Andreev-like tunneling (when two anyons collide) as $P_{\text{Andreev}}^{\text{anyon}}$, leaving $1 - P_{\text{Andreev}}^{\text{anyon}}$ the chance without the Andreev-like tunneling. The modification only exists in the reducible part, leading to

$$\begin{aligned} s_{\text{T}} = \langle \delta \hat{I}_{\text{T}}^2 \rangle &= W_A(1 - W_B)W_C + W_B(1 - W_A)W_C + W_A W_B P_{\text{Andreev}}^{\text{anyon}} - W_C^2(W_A - W_B)^2 \\ &= (W_A + W_B)W_C - (W_A^2 + W_B^2)W_C^2 + W_A W_B P_{\text{Andreev}}^{\text{stat}}, \end{aligned} \quad (\text{S47})$$

where $P_{\text{Andreev}}^{\text{stat}} = P_{\text{Andreev}}^{\text{anyon}} - P_{\text{Andreev}}^{\text{dist}}$ is the function that quantifies the Andreev-like tunneling probability from pure anyonic statistics. Indeed, $P_{\text{Andreev}}^{\text{stat}}$ equals the difference between two functions: (i) the chance of Andreev-like tunneling when two distinguishable anyons collide at the central QPC, $P_{\text{Andreev}}^{\text{dist}} = 2W_C(1 - W_C)$; and (ii) the function $P_{\text{Andreev}}^{\text{anyon}}$ that refers to the Andreev-like tunneling when all anyons are indistinguishable. After removing statistics-irrelevant contributions [first two terms of Eq. (S47), which perfectly equals that in Eq. (S46)], the rest noise discloses the influence of anyonic statistics on Andreev-like tunnelings. Actually, by comparing Eq. (S47) to Eqs. (2) and (3) of the main text, i.e.,

$$\begin{aligned} S_{1A} &= T_C \frac{T_A}{\pi^2} \frac{2\nu \sin^2(\pi\nu) e I_{A0}}{(2 - 3\nu + 2\nu^2)(2 - 4\nu + 2\nu^2)}, \\ S_{1B} &= T_C \frac{T_B}{\pi^2} \frac{2\nu \sin^2(\pi\nu) e I_{B0}}{(2 - 3\nu + 2\nu^2)(2 - 4\nu + 2\nu^2)}, \\ S_2 &= T_C \frac{T_A T_B}{\pi^2} \frac{2\nu \sin^2(\pi\nu) e I_+}{(2 - 5\nu + 4\nu^2)(2 - 6\nu + 4\nu^2)}, \end{aligned} \quad (\text{S48})$$

one immediately notice that $S_{1A} + S_{1B}$ corresponds to the linear term (the first term) of Eq. (S47). Its bilinear term, on the other hand, is captured by S_2 . With this message in mind, and the definition of $\mathcal{P}_{\text{Andreev}}$ in the main text, we can also express $\mathcal{P}_{\text{Andreev}}$ as

$$\mathcal{P}_{\text{Andreev}} = \frac{1}{eI_+} \int d\epsilon W_A W_B P_{\text{Andreev}}^{\text{stat}}(\epsilon). \quad (\text{S49})$$

As another feature, all tunneling current noise expressions do not contain fractional charge ν , as only electrons are allowed to tunnel through the central QPC. As will be shown shortly, this feature greatly contrasts that for cross and auto correlations.

Before ending this subsection, we can obtain values of W_A , W_B , and $P_{\text{Andreev}}^{\text{stat}}$ by comparing Eq. (S47) and Eqs. (2)-(3) of the main text

$$\begin{aligned} W_A &= \frac{h}{e^2} \frac{\partial_V I_{A0}}{\nu}, \quad W_B = \frac{h}{e^2} \frac{\partial_V I_{B0}}{\nu}, \\ P_{\text{Andreev}}^{\text{stat}} &= T_C \frac{T_A T_B}{\pi^2} \frac{e^2}{h} \frac{2\nu \sin^2(\pi\nu)}{(2-5\nu+4\nu^2)(2-6\nu+4\nu^2)} \frac{W_A + W_B}{W_A W_B}, \end{aligned} \quad (\text{S50})$$

where the value of $P_{\text{Andreev}}^{\text{stat}}$ depends on the combination of microscopic tunneling amplitudes, i.e., $(T_A + T_B)T_C$. Here, the dependence on $(T_A + T_B)$ can be removed by dividing the function by the non-equilibrium current $I_+ = I_{A0} + I_{B0} \propto T_A + T_B$.

IVB. Cross correlation noise

Now we move to consider the cross correlation noise. Once again, we start with the distinguishable situation. By distinguishable, we refer to an imagined situation where anyons in A and B are marked out in different ways, and thus being distinguishable from each other. However, tunnelings at the central QPC still resort to Andreev-like tunnelings that accompany reflections of holes with fractional charges. The reducible part of the cross correlation noise then becomes

$$\begin{aligned} \langle \hat{I}_A \hat{I}_B \rangle_{\text{dist}} &= (\nu-1)W_C W_A (1-W_B) + (\nu-1)W_C W_B (1-W_A) \\ &\quad + W_A W_B [P_{\text{Andreev}}^{\text{dist}}(\nu^2-1) + (1-P_{\text{Andreev}}^{\text{dist}})\nu^2] \\ &= (\nu-1)W_C [W_A(1-W_B) + W_B(1-W_A)] + W_A W_B (\nu^2 - P_{\text{Andreev}}^{\text{dist}}), \end{aligned} \quad (\text{S51})$$

while the current average product now equals $\langle \hat{I}_A \rangle \langle \hat{I}_B \rangle = [\nu W_A - W_C(W_A - W_B)][\nu W_B + W_C(W_A - W_B)]$, where the factor of ν refers to the fractional charge of a non-equilibrium anyon, and the factor of “1” in the other term (the term proportional to W_C) refers to the transmission of a full electron across the central QPC. With the reducible noise, and the current average product, we arrive at the irreducible cross correlation noise

$$\langle \delta \hat{I}_A \delta \hat{I}_B \rangle_{\text{dist}} = -(1-\nu)W_C(W_A + W_B) - W_C(\nu - W_C)(W_A^2 + W_B^2), \quad (\text{S52})$$

which, similarly as the tunneling current noise Eq. (S47), does not contain the bilinear contribution $\propto W_A W_B$, and thus can be considered as the summation of two single-particle processes. The second term of Eq. (S52), corresponding to the current average product of single-source situation, has an apparent Andreev tunneling signature: the charge equals ν (corresponding to the non-equilibrium anyon) without charge tunneling, but becomes $\nu - 1$ (corresponding to the reflected hole) after the tunneling.

Now we move to the physical situation, where anyons in edges A and B are indistinguishable, leading to the irreducible cross correlation function

$$\begin{aligned}
s_{AB} &= \langle \delta \hat{I}_A \delta \hat{I}_B \rangle_{\text{anyon}} \\
&= (\nu-1)W_C W_A (1-W_B) + (\nu-1)W_C W_B (1-W_A) \\
&\quad + W_A W_B [P_{\text{Andreev}}^{\text{anyon}} (\nu^2-1) + (1-P_{\text{Andreev}}^{\text{anyon}}) \nu^2] \\
&= (\nu-1)W_C W_A (1-W_B) + (\nu-1)W_C W_B (1-W_A) \\
&\quad + W_A W_B \{ (P_{\text{Andreev}}^{\text{dist}} + P_{\text{Andreev}}^{\text{anyon}} - P_{\text{Andreev}}^{\text{dist}}) (\nu^2-1) \\
&\quad + [1 - (P_{\text{Andreev}}^{\text{dist}} + P_{\text{Andreev}}^{\text{anyon}} - P_{\text{Andreev}}^{\text{dist}})] \nu^2 \} \\
&= (\nu-1)W_C W_A (1-W_B) + (\nu-1)W_C W_B (1-W_A) \\
&\quad + W_A W_B [P_{\text{Andreev}}^{\text{dist}} (\nu^2-1) + (1-P_{\text{Andreev}}^{\text{dist}}) \nu^2] - W_A W_B (P_{\text{Andreev}}^{\text{anyon}} - P_{\text{Andreev}}^{\text{dist}}) \\
&= -(1-\nu)W_C (W_A + W_B) - W_C (\nu - W_C) (W_A^2 + W_B^2) - W_A W_B P_{\text{Andreev}}^{\text{stat}}.
\end{aligned} \tag{S53}$$

Comparison between Eqs. (S47) and (S53) shows that for the leading-contribution, i.e., terms linear in W_A or W_B , the tunneling noise and the cross correlation noise are proportional to each other. This proportionality agrees with the experimental measurement of Ref. [S22]. More importantly, the bilinear term, i.e., the statistics-induced contribution, can be extracted via either tunneling current noise, or the cross correlation: indeed, the obtained statistics-induced noise has only a difference in sign. This result indicates that one can obtain the entanglement pointer of Andreev-like tunnelings, through either tunneling current, or cross correlation noise measurements, whichever is more convenient.

In our previous work Ref. [S23], we define another entanglement pointer \mathcal{P}_E , for the integer situation. With its previous definition, and Eq. (S53) for cross correlation of the anyonic version, we find out that

$$\begin{aligned}
\mathcal{P}_E &= \int d\epsilon s_{AB}(W_A, W_B, \epsilon) - s_{AB}(W_A, 0, \epsilon) - s_{AB}(0, W_B, \epsilon) \\
&= - \int d\epsilon W_A W_B P_{\text{Andreev}}^{\text{stat}}(\epsilon),
\end{aligned} \tag{S54}$$

which is proportional to the integral of the statistics-influenced central factor $P_{\text{Andreev}}^{\text{stat}}$. In addition, since $W_A W_B P_{\text{Andreev}}^{\text{stat}}$ is the only bilinear (in W_A and W_B) term in both S_T and S_{AB} , the function \mathcal{P}_E can also be obtained with tunneling current noise, with only an extra minus sign in definition.

IVC. The auto-correlation

Finally, we move to consider two auto-correlations, $\langle \delta \hat{I}_A^2 \rangle_{\text{anyon}}$ and $\langle \delta \hat{I}_B^2 \rangle_{\text{anyon}}$. Once again, we start with the benchmark scenario where anyons in A are distinguishable

from those in B . In this case, the reducible correlations equal

$$\begin{aligned}
\langle \hat{I}_A^2 \rangle_{\text{dist}} &= \nu^2(1 - W_C)W_A(1 - W_B) + W_C W_B(1 - W_A) + W_C W_A(1 - W_B)(1 - \nu)^2 \\
&+ W_A W_B \left[\frac{P_{\text{Andreev}}^{\text{dist}}}{2}(\nu - 1)^2 + \frac{P_{\text{Andreev}}^{\text{dist}}}{2}(\nu + 1)^2 + (1 - P_{\text{Andreev}}^{\text{dist}})\nu^2 \right] \\
&= \nu^2 W_A(1 - W_B) + W_C [W_B(1 - W_A) + (1 - 2\nu)W_A(1 - W_B)] + W_A W_B (P_{\text{Andreev}}^{\text{dist}} + \nu^2), \\
\langle \hat{I}_B^2 \rangle_{\text{dist}} &= \nu^2(1 - W_C)W_B(1 - W_A) + W_C W_A(1 - W_B) + W_C W_B(1 - W_A)(1 - \nu)^2 \\
&+ W_A W_B \left[\frac{P_{\text{Andreev}}^{\text{dist}}}{2}(\nu - 1)^2 + \frac{P_{\text{Andreev}}^{\text{dist}}}{2}(\nu + 1)^2 + (1 - P_{\text{Andreev}}^{\text{dist}})\nu^2 \right] \\
&= \nu^2 W_B(1 - W_A) + W_C [W_A(1 - W_B) + (1 - 2\nu)W_B(1 - W_A)] + W_A W_B (P_{\text{Andreev}}^{\text{dist}} + \nu^2)
\end{aligned} \tag{S55}$$

We can again use the current averages $\langle \hat{I}_A \rangle = \nu W_A - W_C(W_A - W_B)$ and $\langle \hat{I}_B \rangle = \nu W_B + W_C(W_A - W_B)$, to rewrite the reducible correlations into irreducible ones

$$\begin{aligned}
\langle \delta \hat{I}_A^2 \rangle_{\text{dist}} &= W_A [W_C + \nu(1 - W_A)(\nu - 2W_C)] + W_B W_C - (W_A^2 + W_B^2)W_C^2, \\
\langle \delta \hat{I}_B^2 \rangle_{\text{dist}} &= W_B [W_C + \nu(1 - W_B)(\nu - 2W_C)] + W_A W_C - (W_A^2 + W_B^2)W_C^2,
\end{aligned} \tag{S56}$$

which also display the separation of contributions from different edges. For the situation where all anyons are perfectly indistinguishable, once again only the value of $P_{\text{Andreev}}^{\text{dist}}$ is replaced by $P_{\text{Andreev}}^{\text{anyon}}$, leading to modified auto-correlations

$$\begin{aligned}
s_{AA} &= \langle \delta \hat{I}_A^2 \rangle_{\text{anyon}} = W_A [W_C + \nu(1 - W_A)(\nu - 2W_C)] + W_B W_C \\
&\quad - (W_A^2 + W_B^2)W_C^2 + W_A W_B P_{\text{Andreev}}^{\text{stat}}, \\
s_{BB} &= \langle \delta \hat{I}_B^2 \rangle_{\text{anyon}} = W_B [W_C + \nu(1 - W_B)(\nu - 2W_C)] + W_A W_C \\
&\quad - (W_A^2 + W_B^2)W_C^2 + W_A W_B P_{\text{Andreev}}^{\text{stat}},
\end{aligned} \tag{S57}$$

which contains the same form of the statistical term $W_A W_B P_{\text{Andreev}}^{\text{stat}}$, as that in Eqs. (S47) and (S53), for tunneling current noise and cross correlation, respectively. In addition, the same as cross correlation and tunneling current noise, the only bilinear term of auto correlations equal $W_A W_B P_{\text{Andreev}}^{\text{stat}}$, meaning that $\mathcal{P}_{\text{Andreev}}$ can also be measured with the auto correlation, i.e.,

$$\begin{aligned}
\mathcal{P}_{\text{Andreev}} &= \frac{[S_{\text{T}}(T_A, 0) + S_{\text{T}}(0, T_B) - S_{\text{T}}(T_A, T_B)]}{eI_+} \\
&= -\frac{[S_{AB}(T_A, 0) + S_{AB}(0, T_B) - S_{AB}(T_A, T_B)]}{eI_+} \\
&= \frac{[S_{AA}(T_A, 0) + S_{AA}(0, T_B) - S_{AA}(T_A, T_B)]}{I_+} \\
&= \frac{[S_{BB}(T_A, 0) + S_{BB}(0, T_B) - S_{BB}(T_A, T_B)]}{eI_+},
\end{aligned} \tag{S58}$$

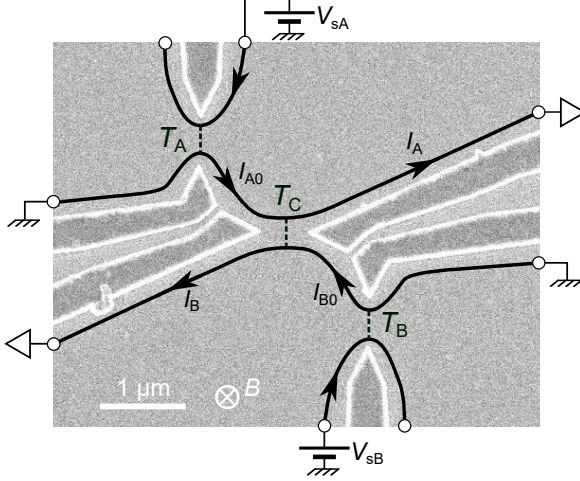


Fig. S2 E-beam micrograph of the experimental device (cf. Ref. [S22]), which is schematically shown in Fig. 1 of the main text. The QPCs are formed by applying negative voltages to metallic gates deposited at the surface (darker with bright edges). The chiral edge channels are displayed as continuous black lines with arrows. The tunneling processes take place along the dashed lines. The source QPCs in subsystems \mathcal{A} and \mathcal{B} are set for $e/3$ quasiparticle tunnelings, whereas the central QPC is tuned to e quasielectron tunnelings. The tunneling quasiparticles are ascertained from shot noise measurements of the tunneling charge, in the presence of a direct voltage bias applied to the considered QPC.

with similar definitions, by removing single-source contributions. Here $S_{AA} \equiv \int dt \langle \delta \hat{I}_A(t) \delta \hat{I}_A(0) \rangle$ and $S_{BB} \equiv \int dt \langle \delta \hat{I}_B(t) \delta \hat{I}_B(0) \rangle$ refer to auto correlations.

V. Experiment

In this section, we briefly describe the experimental setup of Ref. [S22] used to obtain the data, which we analyze in the main text in the context of the theory of entanglement pointer.

The experiment is performed on the Ga(Al)As device shown in Fig. S2 (see Ref. [S22] for details). It is cooled at an electronic temperature of 35 mK and set at the center of the $\nu = 1/3$ fractional quantum Hall plateau. The spectral density of the current auto- and cross-correlations $\langle \delta \hat{I}_A^2 \rangle$, $\langle \delta \hat{I}_B^2 \rangle$ and $\langle \delta \hat{I}_A \delta \hat{I}_B \rangle$ are simultaneously measured around a frequency of 0.86 MHz. The dc currents $I_{A,B,T}$ are obtained by integrating the differential conductances $\partial I_{A,B,T} / \partial V_{sA,sB}$ directly measured by standard lock-in techniques at frequencies below 100 Hz.

Importantly, the present data-theory comparison is performed on a specific data set, which was measured following a protocol optimized to limit as much as possible any changes between the different configurations of the sources. This is essential for the entanglement pointer, which is obtained from the small difference of large signals. Note that the data shown in the main text of Ref. [S22] do not fully follow the procedure described below:

First, the source QPCs are activated not by changing the gate voltage controlling

their transmission parameter $T_{A,B}$ but instead by setting the dc bias voltage $V_{sA,sB}$ to V . Indeed, changing the gate voltage controlling one source (e.g. in branch A) would also change the other transmissions (T_B and T_C) by capacitive crosstalk, and thereby introduce unwanted artifacts in P_{Andreev} . Note that the applied dc bias voltage itself also acts electrostatically on the QPCs. This can play a role, as further discussed in the experiment-theory comparison, yet it is a smaller effect since the bias voltage changes ($V_{sA,sB} \lesssim 0.1$ mV) are much smaller than the gate voltage changes to open or close a QPC (~ 1 V).

Second, the necessary averaging time is split in several sequences alternating between the following successive configurations: (i) source sA is ON and sB is OFF ($V_{sA} = V$, $V_{sB} = 0$), (ii) source sA is OFF and sB is ON ($V_{sA} = 0$, $V_{sB} = V$), (iii) The central QPC is directly voltage biased for tunneling charge characterization, and (iv) sources sA and sB are both ON ($V_{sA} = V_{sB} = V$). This allows us to effectively cancel out in P_{Andreev} the small drifts of the QPCs with time, which could otherwise have a noticeable impact.

VI. Details on the experiment-theory comparison

In this section, we present details of the experiment-theory analysis that leads to Fig. 3 of the main text. To begin with, Fig. 3a shows the raw data from Ref. [S22]. Following Fig. 3a, the sum of the two single-source cross-correlation functions has a larger magnitude than that of the double-source cross correlation. This apparently disagrees with our major results Eqs. (4) and (6), which instead predicts a larger magnitude of the correlation function for the double-source scenario.

The origin of this discrepancy can be understood by noticing Fig. 3b, where the values of the transmission coefficient in the single-source settings clearly deviate from their corresponding double-source values. This deviation is minor and implicit when plotting with V (V_{sA} or V_{sB}); it however becomes manifest if plotting with the total nonequilibrium current I_+ , as in Fig. S3e. This can be attributed to the non-local electrostatic effects present in the setup. Depending on the bias voltages the overall electrostatic potential landscape changes, thus shifting the edges in real space. This shift affects the transparency of the barriers between the edges.

Therefore, in order to compare the single-source and double-source current correlation functions, a rescaling of the double-source transmission is required (see below for detailed steps). In addition, following Fig. S3a, transmission probabilities W_A , W_B greatly deviate from the non-interacting chiral Luttinger liquid prediction (i.e., $W_{A,B} \propto I_+^{(2\nu-2)/(2\nu-1)}$, denoted by the gray dashed line of the inset of Fig. S3a), which implies the energy and/or voltage dependence of the bare transmission probabilities T_A and T_B in the Hamiltonian. In particular, the voltage dependence can be again related to the global electrostatics of the setup. In this work, this dependence is included by working with differential noises.

Below, we list the steps of the data processing that lead to Fig. 4 of the main text. More specifically, Fig. 4 contains four sets of data: the ‘‘theoretical data’’ [obtained from Eq. (3) of the main text], and the rescaling of the experimental data.

Theoretical data:

To obtain the “theoretical data” following Eq. (3) of the main text, one needs to know the tunneling parameters (T_A , T_B and T_C), and the ultraviolet cutoff τ_0 , from the experimental data. Here, we take the following steps.

(i) The effective transmission probabilities $W_A(V_{sA}, V_{sB} = 0)$ and $W_B(V_{sA} = 0, V_{sB})$ for the single-source cases, defined as

$$W_A(V_{sA}, 0) = \frac{\partial I_{A0}}{\partial V_{sA}} \frac{\hbar}{\nu e^2}, \quad W_B(0, V_{sB}) = \frac{\partial I_{B0}}{\partial V_{sB}} \frac{\hbar}{\nu e^2}, \quad (\text{S59})$$

are experimentally obtained by applying a small AC voltage on top of a DC background voltage (shown in Fig. S3b).

(ii) Next, we find the values of $W_C(V_{sA}, V_{sB} = 0)$ and $W_C(V_{sA} = 0, V_{sB})$ for the single-source scenario. These two quantities, defined as

$$W_C(V_{sA}, 0) = \frac{\partial I_T}{\partial I_{A0}} \nu, \quad W_C(0, V_{sB}) = -\frac{\partial I_T}{\partial I_{B0}} \nu, \quad (\text{S60})$$

are also experimentally obtained by applying a weak AC bias on top of a relatively large DC background.

(iii) We obtain the value of the ultraviolet cutoff, with Eq. (S21), or more specifically,

$$\begin{aligned} \tau_0 &= \frac{\hbar}{\nu V_{sA}} \frac{I_T(V_{sA}, 0)}{S_T(V_{sA}, 0)} \frac{2 - 5\nu + 2\nu^2}{2[\nu + W_A(V_{sA}, 0) \sin(2\pi\nu)]} \\ &= \frac{\hbar}{\nu V_{sB}} \frac{I_T(0, V_{sB})}{S_T(0, V_{sB})} \frac{2 - 5\nu + 2\nu^2}{2[\nu + W_B(0, V_{sB}) \sin(2\pi\nu)]}. \end{aligned} \quad (\text{S61})$$

Afterwards, we obtain the values T_A , T_B and T_C , using

$$\begin{aligned} W_A(V_{sA}, 0) &= T_A(V_{sA}, 0) \frac{\sin(2\pi\nu)\Gamma(1-2\nu)}{2\pi^2} \left(\frac{\tau_0 \nu e V_{sA}}{\hbar} \right)^{2\nu-2}, \\ W_B(0, V_{sB}) &= T_B(0, V_{sB}) \frac{\sin(2\pi\nu)\Gamma(1-2\nu)}{2\pi^2} \left(\frac{\tau_0 \nu e V_{sB}}{\hbar} \right)^{2\nu-2}, \\ W_C(V_{sA}, 0) &= T_A(V_{sA}, 0) T_C[I_+(V_{sA})] \frac{2\nu^2 (1 - \cos 2\pi\nu) \left[\nu^2 \frac{e}{\hbar} V_{sA} + \frac{I_{A0}(V_{sA})}{e} \sin 2\pi\nu \right]}{\pi^2 (2-3\nu+2\nu^2)(2-4\nu+2\nu^2)(2-5\nu+2\nu^2)} \tau_0, \\ W_C(0, V_{sB}) &= T_B(0, V_{sB}) T_C[I_+(V_{sB})] \frac{2\nu^2 (1 - \cos 2\pi\nu) \left[\nu^2 \frac{e}{\hbar} V_{sB} + \frac{I_{B0}(V_{sB})}{e} \sin 2\pi\nu \right]}{\pi^2 (2-3\nu+2\nu^2)(2-4\nu+2\nu^2)(2-5\nu+2\nu^2)} \tau_0. \end{aligned} \quad (\text{S62})$$

Notice that in Eq. (S62), all transmission coefficients are expressed as functions of the corresponding voltages. The coefficients T_A , T_B and T_C , which would be constants in a conventional Luttinger liquid theory, depend on voltage through the energy and/or voltage dependence of bare transmission probabilities. This leads to the deviation of the voltage dependencies of currents and noises from the expressions predicted by the Luttinger liquid theory, where voltage enters in the form of an anomalous scaling. With the above procedure, we have thus included the extra (non-Luttinger) voltage dependence of coefficients that appear in the Hamiltonian, (i.e., ζ_A , ζ_B and ζ_C).

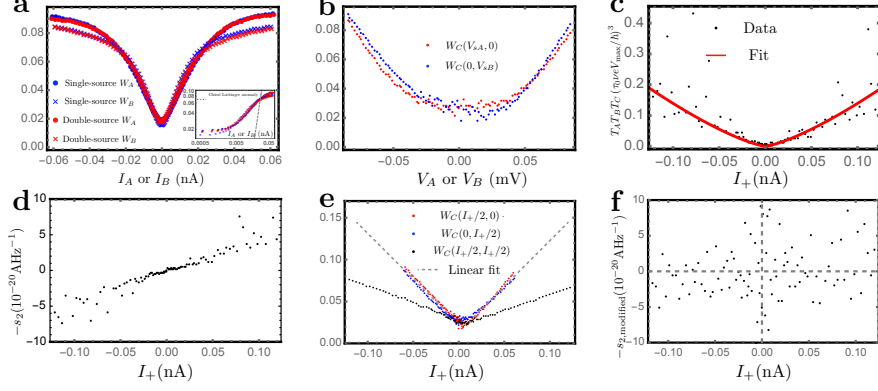


Fig. S3 Data used to obtain Fig. 3c of the main text. **a**, Transmissions W_A and W_B at diluters, for single-source and double-source situations. The x -axis refers to the non-equilibrium current through the corresponding diluter. The single-source and double-source data agrees amazingly with each other. For each value of the non-equilibrium current, W_A and W_B have a small deviation, indicating different barrier amplitudes at upper and lower diluters. **b**, Effective transmission at the central QPC, for single-source settings. **c**, The value $T_A T_B T_C$ obtained from Eq. (S63). When calculating differential noise, we would like to omit contributions from the points that greatly deviate from the fit $\sim I_+^{4/3}$. **d**, The differential noise obtained from Eq. (3) of the main text. Its integral over I_+ leads to blue points of Fig. 3c of the main text. **e**, The linear fit (the gray dashed line) of the transmission probability W_C at the central QPC. **f**, The differential noise, obtained after the rescaling of the double-source noise. It is rather noisy, in comparison to that of **d**. Its integral over I_+ leads to red points of Fig. 3c of the main text.

(iv) To obtain entanglement pointer [given by Eq. (4) of the main text], we also need to know the value of the product $T_A T_B T_C$, with the equality

$$T_A T_B T_C = \sqrt{W_A W_B W_C^2} \frac{\pi^4}{\nu^3} \left(\frac{\tau_0 \nu e V}{\hbar} \right)^{1-2\nu} \frac{(2-3\nu+2\nu^2)(2-4\nu+2\nu^2)(2-5\nu+2\nu^2)}{\sin(2\pi\nu)[1-\cos(2\pi\nu)]\Gamma(1-2\nu)}, \quad (\text{S63})$$

where explicit and implicit dependencies on $V_{sA} = V_{sB} = V$ have been omitted for simplicity. The factor W_C^2 under the square root is the product of two single-source contributions: $W_C^2 = W_C(V, 0)W_C(0, V)$. The dependence of $T_A T_B T_C$ on I_+ is presented by Fig. S3c. To avoid influence from strong fluctuation, we neglect points that greatly deviate from the fitting $\sim I_+^{4/3}$ (red line of Fig. S3c). This dependence of T_A , T_B and T_C , as analyzed at the beginning of this section, leads to the deviation of the $I_+(V)$ dependence predicted by the Luttinger liquid theory (where $I_+ \propto V^{2\nu-1}$). The product $T_A T_B T_C$ obtained this way from the measured data has a meaning of “would-be” product of “virtual” Luttinger-liquid transmission probabilities that would yield the same current at given voltages in the experiment.

(v) We are now ready to calculate the differential noise, which is defined as $s_2(I_+) \equiv \partial_{I_+} S_2(I_+)$ (shown in Fig. S3d). The integral of $s_2(I_+)$ yields the blue points in Fig. 3c of the main text.

Rescaling of the experimental data:

In this part, we will use current as the argument of W_C for clarity of the description of the procedure. We consider the same values of total current I_+ in the single-source (where $I_+ = I_{A0}$ or $I_+ = I_{B0}$) and double-source (where $I_{A0} = I_{B0} = I_+/2$) scenarios.

(i) For a given value of I_+ , read out the data of single-source effective transmission probabilities $W_C(I_+, 0)$ and $W_C(0, I_+)$, following the definition of Eq. (S60). We also obtain the double-source effective transmission amplitudes $W_C(I_+/2, I_+/2)$, defined as

$$W_C(I_+/2, I_+/2) \equiv \nu \frac{\partial I_T(I_+, I_-)}{\partial I_-} \Big|_{I_- = 0}. \quad (\text{S64})$$

Once again, it is experimentally obtained by applying a weak AC voltage on top of a DC background. However, different from single-source scenarios, the measurement of $W_C(I_+/2, I_+/2)$ requires the application of equal AC bias in both sources. For double-source situations, the total non-equilibrium current is larger than that of single-source ones. We thus have to take a linear fit (shown in Fig. S3e), to rescale $W_C(I_+/2, I_+/2)$ for the entire relevant range of I_+ .

(ii) For each value of I_+ , we obtain the differential cross correlation for double-source correlations, i.e., $s_{AB, \text{double}}(I_+) \equiv \partial_{I_+} S_{AB}(I_+/2, I_+/2)$. We then rescale the double source differential noise, following

$$s_{AB, \text{modified}}(I_+) \equiv s_{AB, \text{double}}(I_+) \frac{W_C(I_+, 0) + W_C(0, I_+)}{2W_C(I_+/2, I_+/2)}. \quad (\text{S65})$$

We further use $s_{2, \text{modified}}(I_+) \equiv s_{AB, \text{modified}}(I_+) - s_{AB, \text{single}}(I_+, 0) - s_{AB, \text{single}}(0, I_+)$, where the latter two are the single-source differential noises.

(iii) Finally, we integrate $s_{2, \text{modified}}$ over the relevant current range, to obtain the modified double-source noise

$$S_{AB, \text{modified}}(I_+) \equiv \int_0^{I_+} dI s_{2, \text{modified}}(I). \quad (\text{S66})$$

The plot of the function $s_{2, \text{modified}}(I_+)$ is presented in Fig. S3f.

References

- [S1] C. L. Kane and Matthew P. A. Fisher, ‘‘Transmission through barriers and resonant tunneling in an interacting one-dimensional electron gas,’’ *Phys. Rev. B* **46**, 15233–15262 (1992).
- [S2] Gerald D. Mahan, *Many-particle physics* (Springer, New York, 2000).
- [S3] Henrik Bruus and Karsten Flensberg, *Many-Body Quantum Theory in Condensed Matter Physics: An Introduction*, 2nd ed. (Oxford University Press, London, 2004).

- [S4] Bernd Rosenow, Ivan P. Levkivskiy, and Bertrand I. Halperin, “Current correlations from a mesoscopic anyon collider,” *Phys. Rev. Lett.* **116**, 156802 (2016).
- [S5] June-Young M. Lee and H. S. Sim, “Non-Abelian anyon collider,” *Nature Communications* **13**, 6660 (2022).
- [S6] June-Young M. Lee, Changki Hong, Tomer Alkalay, Noam Schiller, Vladimir Umansky, Moty Heiblum, Yuval Oreg, and H. S. Sim, “Partitioning of diluted anyons reveals their braiding statistics,” *Nature* **617**, 277–281 (2023).
- [S7] Michele Filippone and Piet W. Brouwer, “Tunneling into quantum wires: Regularization of the tunneling Hamiltonian and consistency between free and bosonized fermions,” *Phys. Rev. B* **94**, 235426 (2016).
- [S8] Tom Morel, June-Young M. Lee, H.-S. Sim, and Christophe Mora, “Fractionalization and anyonic statistics in the integer quantum Hall collider,” *Phys. Rev. B* **105**, 075433 (2022).
- [S9] J. Rech, T. Jonckheere, B. Grémaud, and T. Martin, “Negative delta- T noise in the fractional quantum Hall effect,” *Phys. Rev. Lett.* **125**, 086801 (2020).
- [S10] Gu Zhang, Igor V. Gornyi, and Christian Spånslätt, “Delta- T noise for weak tunneling in one-dimensional systems: Interactions versus quantum statistics,” *Phys. Rev. B* **105**, 195423 (2022).
- [S11] Noam Schiller, Yuval Oreg, and Kyrylo Snizhko, “Extracting the scaling dimension of quantum Hall quasiparticles from current correlations,” *Phys. Rev. B* **105**, 165150 (2022).
- [S12] Tomer Alkalay *et al.*, “unpublished; talk by K. Snizhko at “QHEdge-Grenoble,” Villard de Lans, France,” (2023).
- [S13] G. Campagnano, P. Lucignano, and D. Giuliano, “Chirality and current-current correlation in fractional quantum Hall systems,” *Phys. Rev. B* **93**, 075441 (2016).
- [S14] T. Giamarchi, *Quantum Physics in One Dimension* (Oxford Univ. Press, Oxford UK, 2004).
- [S15] I. Safi and H. J. Schulz, “Transport in an inhomogeneous interacting one-dimensional system,” *Phys. Rev. B* **52**, R17040–R17043 (1995).
- [S16] I. Safi, “A dynamic scattering approach for a gated interacting wire,” *The European Physical Journal B - Condensed Matter and Complex Systems* **12**, 451–455 (1999).
- [S17] I.V. Protopopov, Yuval Gefen, and A.D. Mirlin, “Transport in a disordered $\nu = 2/3$ fractional quantum Hall junction,” *Annals of Physics* **385**, 287–327

(2017).

- [S18] C. Spånslätt, Yuval Gefen, I. V. Gornyi, and D. G. Polyakov, “Contacts, equilibration, and interactions in fractional quantum Hall edge transport,” *Phys. Rev. B* **104**, 115416 (2021).
- [S19] Th. Martin and R. Landauer, “Wave-packet approach to noise in multichannel mesoscopic systems,” *Phys. Rev. B* **45**, 1742–1755 (1992).
- [S20] Ya.M. Blanter and M. Büttiker, “Shot noise in mesoscopic conductors,” *Physics Reports* **336**, 1–166 (2000).
- [S21] Gabriele Campagnano, Oded Zilberberg, Igor V. Gornyi, Dmitri E. Feldman, Andrew C. Potter, and Yuval Gefen, “Hanbury Brown–Twiss interference of anyons,” *Phys. Rev. Lett.* **109**, 106802 (2012).
- [S22] P. Glidic, O. Maillet, C. Piquard, A. Aassime, A. Cavanna, Y. Jin, U. Gennser, A. Anthore, and F. Pierre, “Quasiparticle Andreev scattering in the $\nu = 1/3$ fractional quantum Hall regime,” *Nature Communications* **14**, 514 (2023).
- [S23] Gu Zhang, Changki Hong, Tomer Alkalay, Vladimir Umansky, Moty Heiblum, Igor V. Gornyi, and Yuval Gefen, “Measuring statistics-induced entanglement entropy with a Hong-Ou-Mandel interferometer,” (2022), [arXiv:2210.15520](https://arxiv.org/abs/2210.15520) [[cond-mat.mes-hall](https://arxiv.org/abs/2210.15520)] .